NK Cell Exhaustion in Wilson's Disease Revealed by Single-cell RNA Sequencing Predicts the Prognosis of Cholecystitis

Yong Jin[1, #], Jiayu Xing[1, #], Chenyu Dai[2, #], Lei Jin[3, 4], Wanying Zhang[1], Qianqian Tao[3, 4], Mei Hou[1], Ziyi Li[3, 4], Wen Yang[1, 5, *], Qiyu Feng[1, *], Hongyang Wang[1, 5, *] & Qingsheng Yu[2, 3, *]

[1] Cancer Research Center, The First Affiliated Hospital of USTC, Division of Life Sciences and Medicine, University of Science and Technology of China, Hefei, Anhui, 230036, P. R. China.

[2] Department of Cadre Cardiology, The First Affiliated Hospital of Anhui University of Chinese Medicine, Hefei, Anhui, 230031, P. R. China.

[3] Department of General Surgery, The First Affiliated Hospital of Anhui University of Chinese Medicine, Hefei, Anhui, 230031, P. R. China.

[4] Institute of Chinese Medicine Surgery, Anhui Academy of Chinese Medicine, Hefei, Anhui, 230031, P. R. China.

[5] International Co-operation Laboratory on Signal Transduction, Eastern Hepatobiliary Surgery Hospital, Second Military Medical University, Shanghai 200438, China; National Center for Liver Cancer, Second Military Medical University, Shanghai 201805, China.

[#] Contributed equally.

[*] Corresponding author.

Correspondence to Qingsheng Yu (qsy6312@163.com), Hongyang Wang (hywangk@vip.sina.com), or Qiyu Feng (qiyufeng@ustc.edu.cn).

Abstract

Metabolic abnormalities associated with liver disease have a significant impact on the risk and prognosis of cholecystitis. However, the underlying mechanism is complicated and remains to be elucidated. In particular, the effect of metabolic abnormalities on the progression of cholecystitis through the regulation of immune cell function is poorly understood. In this study, we investigated this issue using Wilson's disease (WD) as a model. Wilson's disease is a genetic disorder characterized by impaired mitochondrial function and abnormal copper metabolism. Our retrospective clinical study of over 600 patients with WD found that they have a significantly higher incidence of cholecystitis and a poorer prognosis. The immune cell landscape in the hepatic mesenchymal stromal microenvironment using single-cell RNA sequencing showed that the tissue immune microenvironment is altered in patients with WD, mainly a major change in the constitution and function of the innate immune system, including enhanced antigen presentation process, activation of the immune response, and activation of lymphocytes. Exhaustion of natural killer (NK) cells is the fundamental factor, supported by an increase in the expression of the inhibitory receptors NKG2A and TIGIT and a decrease in the expression of cytotoxic molecules. Clinical tissue and blood samples verified increased $NKG2A^+$ and $TIGIT^+$ NK cells and decreased $IFN\gamma^+$ NK cells in WD. Further bioinformatic analysis has confirmed a positive correlation between NK cell exhaustion and poor prognosis in cholecystitis and other inflammatory diseases. The study demonstrated abnormal function of liver mesenchymal immune cells triggered by specific metabolic dysfunction in WD, with a focus on the correlation between NK cell exhaustion and poor healing of cholecystitis. Our findings highlight the immune cell dysfunction due to metabolic changes in hepatocytes and provide new insights into the improvement of inflammatory diseases by assessing immune cell function.

Keywords: NK cell exhaustion, immune cell dysfunction, metabolic abnormalities, Wilson's disease, cholecystitis

Introduction

Cholecystitis refers to a group of inflammatory diseases with different etiologies and clinical courses[1]. While the corresponding pathological mechanisms of cholecystitis are complicated, systemic inflammation is widely recognized as a primary catalyst of cholecystitis pathology[2-6]. Cholecystectomy is typically the preferred treatment option for patients with severe cholecystitis and gallstones, whereas medication is prescribed for those with mildly symptomatic cholecystitis or calculous cholecystitis. However, the effectiveness of alternative or conservative treatments can vary greatly. Furthermore, a substantial percentage of patients face the possibility of complications or recurrence[7,8]. Therefore, it is important to assess the prognosis of pharmacological treatment in patients with cholecystitis through prospective evaluation. Inflammatory diseases, ranging from common inflammatory patterns to rare chronic illnesses, are characterized by a defective immune system and an exaggerated inflammatory cascade response. Compelling evidence supports that the proportion, gene expression profile, and functional status of immune cells hold significant prognostic value[9-14]. Therefore, it is critical to comprehensively comprehend the immune cell dysfunction linked with cholecystitis, its corresponding altered characteristics, and their prognostic implications.

Natural killer (NK) cells are the major innate lymphocyte subset and are found in most organs[15,16]. They produce lytic granules that eliminate infected or cancerous cells, coordinate the inflammation process, form immunological memory, and modulate antigen-presenting cell function in inflammatory diseases[17-19]. In the context of tumors and chronic infections, NK cells exhibit an exhausted phenotype, termed NK cell exhaustion, which is characterized by downregulated expression of activating receptors (e.g., NKG2D, CD16), upregulated expression of inhibitory receptors (e.g., NKG2A, PD-1, TIGIT, Tim-3), decreased production of effector cytokines, and impaired cytolytic activity[20,21]. Recently, blockade of NKG2A and TIGIT has been shown to reverse NK cell exhaustion and enhance the therapeutic effects of anti-tumor and anti-infective immunotherapies[21-23]. In addition, NK cell exhaustion has been reported to predict poor prognosis in hepatocellular carcinoma and acute myeloid leukemia; however, the correlation of NK cell exhaustion with prognosis in cholecystitis and other inflammatory diseases remains largely unexplored[24-26].

The liver plays a critical role in immune defense. It contains a substantial population of diverse immune

cells, particularly NK cells[27-29]. The liver modulates these cells to mount immune responses upon encountering specific inflammatory triggers[28,30]. Furthermore, liver pathologies affect mesenchymal immune cell function by means of regulating intercellular signaling, thereby influencing systemic inflammatory responses. Liver disease commonly impacts the development and outcome of inflammation-associated diseases such as cholecystitis[31-33]. Wilson's disease (WD) is a rare genetic disorder caused by mutations in the gene encoding the transmembrane copper-transporting P-type ATPase protein[34]. It leads to deficits in mitochondrial structure and function, as well as specific alterations in liver metabolism, resulting in a variety of liver diseases. Additionally, WD is commonly associated with inflammatory conditions in the clinic[35-38]. Thus, WD, with its unique etiology, serves as an excellent model for exploring the regulation of immune cell function by hepatic metabolic abnormalities.

In this retrospective clinical study of over six hundred WD patients, it was found that they had a significantly higher cholecystitis incidence than the general population. This, in turn, is associated with a poor prognosis for cholecystitis in these patients. A thorough examination of the immune cell landscape in the hepatic mesenchymal stromal microenvironment using single-cell RNA sequencing (scRNA-seq) revealed that the tissue immune microenvironment is altered in patients with WD. Specifically, there were significant changes in the composition and function of the innate immune system, including an increase of mononuclear phagocytes (MPs) and NK cells, as well as enhanced pro-inflammatory characteristics. Additionally, there was an enhancement in the biological processes of antigen presentation, activation of immune response, and activation of lymphocytes. One key event among these changes was the exhaustion of NK cells, as demonstrated by an increase in the expression of inhibitory receptors NKG2A and TIGIT and a decrease in the expression of cytotoxic molecules. Multiplex immunohistochemistry and flow cytometry techniques confirmed the exhaustion of NK cells in both clinical liver tissue and peripheral blood samples. Finally, our bioinformatics analysis has confirmed a positive correlation between NK cell exhaustion and poor prognosis in cholecystitis and other inflammatory diseases. Our study has demonstrated abnormal liver mesenchymal immune cell function triggered by specific metabolic dysfunction in WD, focusing on NK cell exhaustion and its correlation with poor healing of cholecystitis. These findings provide foundation for further studies of effect of hepatocytes metabolic changes on

immune cell function and insights into improvement of inflammatory diseases by assessing immune cell function.

Results

WD causes poor prognosis of cholecystitis

WD is a genetic disorder resulting from mutations in the *ATP7B* gene, exhibiting significant genetic heterogeneity with over 600 mutations or polymorphisms[39]. Through sequencing DNA samples from 20 patients with WD, we found that c. 2333G>T (p. R778L) accounted for the majority (65%) of the three most common mutations in Chinese, while c. 2804C>T (p. T935M) and c. 2975C>T (p. P992L) were not detected (Figure 1a)[40]. In hepatocytes, ATP7B deficiency in the trans-Golgi network (TGN) leads to abnormalities in mitochondrial function and copper metabolism, and ultimately to a wide range of liver diseases (Figure 1b)[41-44]. Typical clinical manifestations are liver fibrosis and Kayser-Fleischer Ring in the cornea that caused by Cu accumulation in the cornea (Figure 1c, d)[41]. Additionally, metabolic symptoms of WD patients, such as a higher plasma total cholesterol (T-CHOL) concentration and a lower risk of hyperglycemia (Cohort 1 and Cohort 2), are observed (Figure 1e, Figure S1a). Mitochondrial stress and glycolysis assays revealed that knockout of the *ATP7B* (ATP7B-KO) in human hepatocyte cell lines WRL 68 significantly impaired the basal oxygen consumption rate (OCR) and capacity of ATP production, while the extracellular acidification rate (ECAR) of glycolysis was slightly increased and glycolysis capacity remained unchanged (Figure S1b, c). These results demonstrate that WD is a disease characterized by abnormal hepatocyte metabolism.

Interestingly, chronic cholecystitis emerged as the most common complication, with a notably higher incidence in WD patients (49.51%) compared to HBV patients (9.46%) in Cohort 2 (Figure 1e). Despite the comparable incidence of gallbladder in the two groups and the significantly reduced plasma concentration of total bilirubin in WD patients (Cohort 1 and Cohort 2), this finding holds (Figure 1e). Moreover, in cholecystitis patients, the proportion of cases with abnormal index was significantly higher when combined with WD, which included white blood cell (WBC), neutrophil (NEU), and lymphocyte (LYM) counts (Cohort 3, Figure 1e). Overall, these findings suggest that cholecystitis outcomes are

negatively affected by WD and that there are immune abnormalities that affect the prognosis of cholecystitis in WD patients.

Single-cell profiling of non-parenchymal cells in the liver of WD patients

The hepatic mesenchymal cells from three WD patients and three liver hemangioma patients were analyzed using the 10X Genomics platform for scRNA-seq (Figure 2a) to better understand the complicated immune abnormalities in WD patients. 57,384 high-quality single transcriptomes were generated, with 30,068 cells in the case group and 27,316 in the control group. We validated twenty-six principal components *via* PCA and substantiated the grouping through UMAP dimensionality reduction cluster graph (Figure 2b, c, Figure S2a). We then utilized individual cell expression profiles and reference to cell marker gene expression to implement an automated annotation method, which was further complemented by manual review and fine-tuning. This initial annotation process resulted in the classification and display of 12 significant cell clusters. The UMAP algorithm was used to segregate and display the clusters. The study identified various cell types, including hepatocytes[45,46], cholangiocytes[45], endothelial cells (ECs)[47-49], hepatic stellate cells (HepSCs)[46,50], proliferating cells[48,51,52], B cells[53,54], plasma cells[52,53], T and NK cells[53,55], neutrophils[56], mast cells[48,55,56], mononuclear phagocytes (MPs)[57], and plasmacytoid dendritic cells (pDCs)[48,58] (Figure 2d, e and Figure S2b, c). Figure S2d exhibited the top 10 differently expressed genes (DEGs) for each cell type.

Based on the initial annotation, there were notable variations in the quantities and ratios of different cell types between the case group and control group. Our study observed that T and NK lineages were the primary immune cell population among all the examined samples, accounting for 56.54% in CASE and 73.55% in CON, followed by MPs which constituted 17.33% in CASE and 9.97% in CON (Figure 2f, Figure S2e, and Supplementary Table S1). The significant increase in the proportion of MPs and decrease in T and NK cells suggest that MPs likely dominate the immune microenvironment remodeling in patients with WD, while lymphocytes play a minor role. B cell proportions (4.53% in CASE and 2.27% in CON), plasma cell proportions (2.36% in CASE and 0.42% in CON), and pDC proportions (0.42% in CASE and 0.16% in CON) were elevated, while neutrophil proportions (3.53% in CASE and 6.45% in CON) declined.

The proportion of remaining cells is shown in Supplementary Table S1.

The immune microenvironment was altered in WD patients

To demonstrate dissimilarities in the composition of the immune microenvironment between the two groups of individuals in a more detailed manner, a secondary subtype clustering and annotation process was applied to MPs and T and NK cells (Figure 3a, b, and Figure S3a, b). MPs are myeloid immune cells that serve phagocytic and antigen-presenting functions. These cells, which include monocytes, macrophages, and dendritic cells, play an essential role in determining the nature of the immune response[59]. A total of 6,962 MPs were identified (4,439 in CASE and 2,523 in CON), and they were subdivided into 7 clusters through annotation (Figure 3a, Figure S3a, and Supplementary Table S1). Cell marker genes for annotating cell subtypes were depicted in Figure S3c and d, and Figure S3e demonstrated the top 10 DEGs between the two groups[46,48,49,51,52,55-58,60-65]. The DEGs were related to various cell types, including proliferating cells, macrophages, monocytes, mature dendritic cells (MatureDCs), conventional type 1 dendritic cells (cDC1), conventional type 2 dendritic cells (cDC2), and Kupffer cells (KCs). In the case group, there was a significant increase in both macrophages (25.03% in CASE versus 14.33% in CON) and KCs, the resident macrophages in the liver (26.03% in CASE versus 22.96% in CON), suggesting their involvement in promoting hepatic inflammation in metabolic liver disease (Figure 3a)[66]. By contrast, the percentages of monocytes (35.45% in CASE and 41.78% in CON), cDC1 (2.14% in CASE and 5.99% in CON), and cDC2 (10.39% in CASE and 14.13% in CON) were decreased in the case group (Figure 3a).

Seventeen clusters were obtained through reclustering for the largest population of T and NK cells, totaling 34,339 cells (15,403 cells in CASE and 18,936 in CON)[53,56,67-82]. The clusters included ILC3_IL1R1, NKT_GNLY, NKT_IFNG, NKT_KLRG1, NK_FCER1G, NK_KLRC1, NKT_XCL2, NK_FCGR3A, CD4NaiveT_CCR7, CD4Tmem_CD40LG, CD4Treg_CTLA4, CD8MAIT_KLRB1, CD8MAIT_SLC4A10, CD8Teff_GZMH, CD8Teff_GZMK, CD8Teff_ISG15, and CD8Teff_MT1X (Figure 3b, Figure S3b, Supplementary Table S1). The proportion of NK cells (40.97% and 17.07% in CASE and CON, respectively) and CD4Treg (0.92% and 0.31% in CASE and CON, respectively) was significantly increased in the case group. On the other hand, a decrease of NKT cells (28.72% in CASE and 35.26% in CON),

CD8MAIT (7.76% in CASE and 22.14% in CON) and CD8Teff (14.95% in CASE and 17.88% in CON) was observed in the case group. CD4 regulatory T cells are thought to inhibit T cell activation in autoimmune and virus-related liver diseases, indicating a correlation between elevated CD4 regulatory T cells and reduced CD8 T cells in WD patients[83]. The distribution of other types of cells between the two groups is shown in Figure 3b and Supplementary Table S1.

To systematically evaluate the key functional alteration, we analyzed the top 20 differently expressed genes in all immune cell populations. We found that the expression of genes encoding complement C1q (*C1QA*, *C1QB*, and *C1QC*) and *HLA-DRA* was significantly upregulated in the case group. Conversely, the expression of genes encoding heat shock protein (*HSPA1A*, *HSPA1B*, *HSPM1*, *HSPA6*, *HSP90AB1*, *HSPE1*, and *HSPD1*) was markedly downregulated in the case group (Figure 3c). The Gene Ontology (GO) analysis results demonstrate that WD enhances the abilities of antigen-presenting cells to activate immune response and related lymphocytes, through upregulating antigen processing and presentation, activation of immune response, and positive regulation of lymphocyte activation. However, heat shock proteins delivering antigens may be responsible for the downregulation of lymphocytes differentiation and T cell activation[84]. Next, we analyzed the cellular communication network using Cellchat. Our findings reveal that CD8Teff, KCs, NKT, CD8MAIT, and monocytes were the primary partners in intercellular communication (Figure 3e). Furthermore, CD8Teff and NK cells showed stronger signals in the case group, while neutrophils exhibited weaker signals, in both outgoing and incoming (Figure 3e). Collectively, these results demonstrate that the immune microenvironment in the liver of WD patients is remodeled, with an obvious enhancement in both quantity and function of innate immunocytes.

The dysfunction of main immune cells in WD patients

To obtain a detail analysis of function comparison in immune cells between two groups, we scored and evaluated the core functional signature of major cell types. We further clustered macrophages, which accounted for 14.33% of the MPs in the control group and increased to 25.03% in the case group, resulting in the identification of four distinct subtypes (Figure S4a). Interestingly, these four subtypes in the patients with WD exhibited distinct gene expression profiles. Macrophages_3 in WD displayed elevated

expression levels of S100A family genes (*S100A8*, *S100A9*, *S100A12*, *S100A6*, *VCAN*, *FCN1*, and *S100A4*), indicating a potential contribution to MDSC-like macrophages. In contrast, Macrophages_4 in WD were characterized by upregulation of lipid metabolism genes (*FABP5*, *APOC1*, *CTSD*, and *PLA2G7*) (Figure S4b)[85,86]. By scoring various gene signatures, we compared the M1 polarization, M2 polarization, pro-inflammatory signature, and interferon response signature of four subtypes within two groups (Figure 4a). These four subtypes displayed consistently overlapped M1/M2 signatures. Significantly, the Macrophages_3 subtype exhibited a more pronounced pro-inflammatory signal in the case group, while the other subtypes showed a slight decrease. In addition, the interferon response signature showed slight elevation in four subtypes within the case group. Kupffer cells, which are liver-resident macrophages with unique functions in maintaining homeostasis, represent the most abundant population of tissue-resident macrophages in the human body[66]. KCs were also further clustered and three subtypes were obtained (Figure S4c). Significant differential expression of genes related to the inflammatory response, including *IL1B*, *CXCL2*, *CCL3C1*, *CXCL8*, and *CCL2*, were identified between the two groups (Figure S4d). Similarly, KCs subtypes in two groups also showed overlapping M1/M2 signatures, but all subtypes in the case group showed varying degrees of increase in pro-inflammatory and interferon-responsive signatures (Figure 4b).

Neutrophils, the most abundant leukocytes in human blood, respond to inflammatory stimuli by migrating to the site of inflammation. Its immunological functions, such as phagocytosis, reactive oxygen species generation, degranulation, and production of cytokines and chemokines, play a crucial role in the resolution of inflammation and tissue repair[87,88]. In the case group, a lower percentage of neutrophils (3.53% in CASE and 6.45% in CON) was observed, and the functional characteristics were subsequently evaluated. The results showed that the maturation, chemotaxis, phagocytosis, and chemokine activity scores were decreased in the CASE group, while the activation of the type I interferon signaling pathway was enhanced (Figure 4c).

Since the biological process of antigen processing and presentation was upregulated, we calculated the relative expression intensity of genes encoding MHC molecules and complement molecules in cDC1, cDC2, and mature DCs (Figure 4d). Notably, genes encoding MHC class I molecules (*HLA-A*, *-B*, *-C*, *-E*, and *-F*)

were significantly upregulated in the mature DCs in the case group, while genes encoding MHC class II molecules (*HLA-DQA1*, *-DQA2*, *-DQB1*, *-DQB2*, *-DPA1*, *-DPB1*, *-DRA*, *-DRB1*, and *-DRB5*) were all downregulated in the mature DCs. Monocytes accounted for the highest proportion (35.45% in CASE and 41.78% in CON), and most of them were $CD14^+$ classical monocytes (Figure S4e). Compared to the control group, *S100A8*, *S100A9*, and *S100A12* were the top 3 upregulated genes in classical monocytes of WD patients (Figure S4f). *S100A8* and *S100A9* are confirmed to play vital roles in modulating the inflammatory responses by recruiting leukocytes and inducing cytokine secretion during inflammation, and as an alarmin, their elevation indicates inflammation in the local environment[89,90]. GO analysis of DEGs in monocytes showed a decrease in biological processes involving cytokine production, response to lipopolysaccharide and bacteria, as well as lymphocyte activation (Figure 4e).

For T cells, we performed GO analysis on DEGs in CD8 T cells between two groups. Notably, the biological processes linked to energy and lipid metabolism were upregulated in several subtypes, including CD4Tmem_CD40LG, CD4Treg_CTLA4, CD8MAIT_KLRB1, CD8MAIT_SLC4A10, CD8Teff_GZMH, and CD8Teff_GZMK. In addition, biological processes associated with response to copper ion were upregulated in the CD8Teff_MT1X subtype (Figure S4g). Meanwhile, T cell subtypes showed comparable cytotoxicity scores, and there were slight changes between two groups (Figure 4f). However, CD8 T cells in the case group exhibited lower levels of exhaustion, except for CD8Teff_GZMH and CD8Teff_ISG15 (Figure 4f). It was also discovered that while the proportion of CD4Treg_CTAL4 was increased in the case group, the Treg signature was slightly lower (Figure 4g). Therefore, these results suggest that WD patients exhibit variations in immune cell function and certain biological processes.

NK cell exhaustion in WD patients

The KEGG analysis of DEGs in NK cells between the case and control groups revealed down-regulation of the natural killer cell-mediated cytotoxicity, along with the NF-kappa B signaling pathway and chemokine signaling pathway, in the case group (Figure S5a). Interestingly, GO analysis showed upregulated biological processes of oxidative phosphorylation and ATP metabolic process, implying the altered metabolic program in NK cells and immune microenvironment (Figure S5b). Since the primary effect of

NK cells is cytotoxicity on target cells, we compared the gene expression levels of activating receptors, inhibitory receptors, and effector molecules between two groups. The results showed increased expression in *KLRC1* and *TIGIT*, and decreased expression in *FCGR3A*, *TNF*, *IFNG*, *GZMB*, *GNLY*, and *CCL4* (Figure 5a). KLRC1 and TIGIT are inhibitory receptors expressed on NK cell surface, and their activation inhibits NK cell functions[21,91]. It was collectively indicated that WD patients have NK cells with exhausted status, which results in poor effector function.

In addition, trajectory analysis showed that NK cells in two groups exhibited a distinct differentiation trajectory. Most of the NK cells in the control group differentiated towards cell fate 1, while those in the case group displayed a higher tendency for differentiation towards cell fate 2, with cell grouping occurring at the final stage (Figure 5b). To ascertain the gene expression profile and the respective cell statuses of the two outcomes, we conducted pseudotime analysis of gene expression in two differentiating directions. The results showed that the gene expression of *KLRC1* (included in gene cluster 1) was gradually increased along the way to cell fate 2, while the gene expression of *FCGR3A*, *TNF*, and *GZMB* (included in gene cluster 3) was weakened in the same direction, suggesting that cell fate 2 is a more exhausted state of NK cells (Figure S5c). Consequently, these results demonstrate that NK cells differentiate towards an exhausted status in WD patients. The development, maturation, and function of NK cells are strictly regulated by transcription factors (TFs)[92]. Next, to assess the transcription factors (TFs) underlying differences in NK cells between WD patients and control groups, we applied PYSCENIC analysis in NK cells. We found that the gene expression of T-bet (encoded by *TBX21*) was downregulated and Eomes (encoded by *EOMES*) was upregulated in the case group (Figure S5d). These two constitute a pair of TFs that play significantly complementary roles in directing the transcriptional program of NK cells. Consistent with previous studies, T-bet expression was downregulated in exhausted NK cells, whereas Eomes expression was increased[24,93,94]. Thus, it was suggested that the downregulation of *TBX21* and upregulation of *EOMES* contributed to the exhaustion of NK cells in WD patients.

To validate NK cell exhaustion in WD patients, we performed multiplex immunohistochemistry (mIHC) staining on liver tissue sections. The results indicate that NKG2A^{+} cells were more frequently observed in CD56^{+} NK cells in WD patients (Figure 5c). Moreover, flow cytometry also confirmed a significant

increase in the percentage of NKG2A^{+} and TIGIT^{+} NK cells and a significant decrease in the percentage of IFNγ^{+} NK cells in peripheral blood lymphocytes from WD patients compared to control groups (Figure 5d, e). Meanwhile, the proportion of NK cells in lymphocytes from peripheral blood and the proportion of CD56^{Bright} NK cells in total NK cells were also calculated. The significantly higher proportion of NK cells in WD patients was consistent with the scRNA sequencing data, and more CD56^{Bright} NK cells suggested a relatively weaker effector function in WD patients (Figure S5e). Therefore, these results indicated that, despite the increased proportion and the upregulated oxidative phosphorylation, NK cell exhibited exhausted status in WD patients.

NK cell exhaustion predicts poor prognosis of cholecystitis

Cholecystitis patients with WD exhibit poorer clinical outcomes. There is evidence demonstrating that NK cell exhaustion is correlated with poor liver cancer prognosis[24,26,95]. Thus, we hypothesize that NK cell exhaustion also contributes to the worse prognosis of cholecystitis patients with WD.

Prognostic models for inflammatory related diseases in GEO were developed using machine learning methods, including random survival forest, ROC curve, and Kaplan-Meier survival curves. A logistic regression algorithm was used to construct a multigene prediction model based on GSE166915 (cholecystitis) and other inflammatory diseases, namely GSE91035 (pancreatitis), GSE75037 (lung adenocarcinoma), and GSE41804 (hepatocellular carcinoma). Using stepwise regression analysis, 12 genes, *KLRC1*, *TIGIT*, *HAVCR2*, *PDCD1*, *CD96*, *LAG3*, *FCGR3A*, *NCR3*, *NCR2*, *NCR1*, *KLRK1*, and *PRF1*, were selected to obtain the best model. The results showed that the predictive model constructed from these genes had good prognostic performance, with AUC of 0.77, 0.80, 0.97, 0.90 (Figure S6a-d). The AUCs of the models in GSE75037 and GSE41084 were relatively high, 0.97 and 0.90, respectively.

Univariate Cox regression analysis revealed that the *TIGIT* (in GSE166915) and *PDCD1* (in GSE75037) were risk genes with hazard ratio (HR) > 1, while *NCR2* (in GSE91035), *HAVCR2*, *KLRC1*, *NCR3* (in GSE75037), *NCR3*, *LAG3* (in GSE41804) were protective gene with HR < 1 among 12 differently expressed markers of NK cell exhaustion (Figure S6a-d). Consistently, the Kaplan-Meier survival curves suggested a shorter survival time in the group with high markers of NK cell exhaustion than in the group

with low markers in the GSE166915 (*P*= 6.1e-6), GSE91035 (*P*= 1.9e-5), GSE75037 (*P*= 3.8e-16), and GSE41804 (*P*= 3.0e-3) datasets (Figure 6a-d). Patients with cholecystitis, pancreatitis, lung adenocarcinoma, and hepatocellular carcinoma who show high markers of NK cell exhaustion are associated with poor survival compared to those with low markers of NK cell exhaustion.

Discussion

Immune cell dysfunction impacts the development, progression, and prognosis of diseases and serves as the basis for immunotherapy. The current understanding of immune cell dysfunction in inflammatory diseases is limited, which hinders the development of effective therapeutic strategies. Our retrospective clinical analysis indicates that WD contributes to the unfavorable prognosis of cholecystitis. We developed an atlas of immune cell dysfunction linked to specific metabolic disruption in WD patients, including 19 major cell types. The immune microenvironment change primarily encompasses increased proportion and strengthened function in innate immunocytes, including upregulated antigen processing and presentation and activation of immune responses. Furthermore, we conducted a comprehensive assessment and comparison of immune cell function in WD and control group. This includes an evaluation of pro-inflammatory and immune regulatory function in macrophages and KCs, phagocytosis and chemokine activity in neutrophils, and cytotoxicity in T cells, etc. We identified NK cell exhaustion in the WD group, with upregulation of *NKG2A* and *TIGIT* and downregulation of *CD16*, *TNF*, *IFNG*, *GZMB*, *GNLY*, and *CCL4*. The validation of our findings in patient liver tissues and blood samples was conducted using immunohistochemistry assays and flow cytometry. Our findings indicated that the NK cell exhaustion signature has the ability to predict and prognosticate inflammatory diseases such as cholecystitis, pancreatitis, lung adenocarcinoma, and hepatocellular carcinoma. These results unveil novel perspectives on the immune cell dysfunction role in inflammatory diseases.

WD represents a model of metabolic abnormality in hepatocytes caused by *ATP7B* mutation. Therefore, immune cell dysfunction was induced by the extracellular signals within the reshaped tissue microenvironment. Emerging research indicates that metabolic crosstalk in the tumor microenvironment disrupts metabolic and signaling pathways in immune cells, leading to dysfunction[96-100]. Targeting metabolic pathways to enhance the efficacy of immunotherapy is a promising approach. Our study found

multiple metabolic abnormalities in immune cells, including the widely upregulated ATP metabolic process in T and NK cells. Interestingly, glycolysis and oxidative phosphorylation contribute to maintain the cytotoxic ability and promote expansion of NK cells[101-103]. However, high rate of oxidative phosphorylation, increased proportion, and exhausted status were simultaneously observed in NK cells of WD patients. Further studies are needed to elucidate the metabolic landscape, mechanisms underlying metabolic alterations, and their role in immune cell dysfunction. Defective ATP7B leads to excessive copper accumulation in the system's circulation. A recent study showed that excess copper induces cell death in a manner dependent on mitochondrial respiration[104]. Considering the impact on mitochondrial respiration processes in immune cells, it is worth investigating the role of copper in the physiology of immune cells. Further research is expected to establish a foundation for improving immunotherapies through metabolic or ionophore interventions.

Methods

Patients and clinical samples

All the clinical data were obtained from The First Affiliated Hospital of Anhui University of Chinese Medicine. The whole blood samples and liver tissue samples were collected from patients at The First Affiliated Hospital of Anhui University of Chinese Medicine. The study was approved by the Ethics Committee of the First Affiliated Hospital of Anhui University of Traditional Chinese Medicine and the Ethics Committee of the First Affiliated Hospital of USTC.

Sanger sequencing

The sanger sequencing on 20 WD patients were conducted by Sangon Biotech (Shanghai) Co., Ltd.

The primers to detect mutations are:

R778L-F, 5'-AGCCTTCACTGTCCTTGTCTTTC-3';

R778L-R, 5'-ATTAGCTGGGATTTCAGAAGTAGTG-3';

T935M-F, 5'-ATGCTTGTGGTGTTTTATTTCTTC-3';

T935M-R, 5'-AGAAGCAAGCAAATAAAATGTAATG-3';

P992L-F, 5'-TCTCAACCTGCCTCTGACTCTG-3';

P992L-R, 5'-TGGTGGCTACTCTGTTGCTACTG-3'.

Cell culture, gene knockout, and metabolic assays

WRL 68 cells were cultured using DMEM high-glucose media supplemented with 10% FBS at 37 °C with 5% CO_2. The lentivirus-mediated CRISPR-Cas9 KO vector targeting human *ATP7B* was obtained from OBiO Technology (Shanghai) Co., Ltd. Cells at 30% to 40% confluency were incubated in a medium containing optimal dilutions of lentivirus, then subjected to puromycin selection to obtain the stable transfected cells. OCRs and ECARs were measured using Seahorse XF Cell Mito Stress Test Kit (103015-100, Agilent) and Seahorse XF Glycolysis Stress Test Kit (103020-100, Agilent) according to manuals in Agilent XFe96 Analyzer, respectively.

Single-cell RNA sequencing

In the cell preparation section: For the quality check and counting of single cell suspension, the cell survival rate is generally above 80%. The cells that have passed the test are washed and resuspended to prepare a suitable cell concentration of 700~1,200 cells/μL for 10x Genomics ChromiumTM. The system is operated on the machine.

Steps in GEM Creation & Thermal cycling: GEMs (Gel Bead in Emulsion) were constructed for single cell separation according to the number of cells to be harvested. After GEMs were normally formed, GEMs were collected for reverse transcription in a PCR machine for labeling.

Post Cycling Cleanup & cDNA Amplication: The GEMs were oil-treated, and the amplified cDNA was purified by magnetic beads, and then subjected to cDNA amplification and quality inspection.

Library Preparation & Quantification: The 3’Gene Expression Library was constructed with the quality-qualified cDNA. After fragmentation, adaptor ligation, sample index PCR, etc., the library is finally quantitatively examined.

Sequencing: The final library pool was sequenced on the Illumina Hiseq instrument using 150-base-pair paired-end reads.

Cell type annotation and differentially expressed genes (DEGs) analysis

The cell type identity of each cluster was determined with the expression of canonical markers found in the DEGs using SynEcoSys database. The markers and references are shown in Supplementary Table S4. To identify DEGs, we used the Seurat FindMarkers function based on Wilcox likelihood-ratio test with default parameters, and selected the genes expressed in more than 10% of the cells in a cluster and with an average log (Fold Change) value greater than 0.25 as DEGs. For the cell type annotation of each cluster, we combined the expression of canonical markers found in the DEGs with knowledge from literatures, and displayed the expression of markers of each cell type with heatmaps that were generated with Seurat Heatmap function. Doublet cells were identified as expressing markers for different cell types, and removed manually.

Pathway enrichment analysis

To investigate the potential functions of DEGs, the Gene Ontology (GO) and Kyoto Encyclopedia of Genes and Genomes (KEGG) analysis were used with the "clusterProfiler" R package 3.16.1[105]. Pathways with p_adj value less than 0.05 were considered as significantly enriched. Gene Ontology gene sets including molecular function (MF), biological process (BP), and cellular component (CC) categories were used as reference.

Cell-cell Interaction Analysis

CellChat (version 0.0.2) was used to analyze the intercellular communication networks from scRNA-seq data[106]. A CellChat object was created using the R package process. Cell information was added into the meta slot of the object. The ligand-receptor interaction database was set, and the matching receptor inference calculation was performed.

Trajectory analysis

Cell differentiation trajectory was reconstructed with Monocle2[107]. Highly-variable genes (HVGs) were used to sort cells in order of spatial-temporal differentiation. We used DDRTree to perform FindVairableFeatures and dimension-reduction. Finally, the trajectory was visualized by plot_cell_trajectory function. Next, CytoTRACE (a computational method that predicts the differentiation state of cells from single-cell RNA-sequencing data using gene Counts and Expression) was used to predict the differentiation potential[108].

Transcription factor regulatory network analysis

Transcription factor network was constructed by pyscenic v0.11.0 using scRNA expression matrix and transcription factors in AnimalTFDB[109]. First, GRNBoost2 predicted a regulatory network based on the co-expression of regulators and targets. CisTarget was then applied to exclude indirect targets and to search transcription factor binding motifs. After that, AUCell was used for regulon activity quantification for every cell.

UCell gene set scoring

Gene set scoring was performed using the R package UCell v 1.1.0[110]. UCell scores are based on the Mann-Whitney U statistic by ranking query genes in order of their expression levels in individual cells. Because UCell is a rank-based scoring method, it is suitable to be used in large datasets containing multiple samples and batches. The gene sets for signature scoring are listed in Supplementary Table S3.

Multiplex immunohistochemistry

The procedure of deparaffinization, dehydration, antigen retrieval, endogenous peroxidases quench, block, antibody incubation was conducted as standard immunohistochemistry. Solution of tyramide signal amplification (TSA) (WAS1101010, BioMed World) was applied on the slides and antibodies were removed by microwave heating. Repeat block, antibody incubation, TSA, and microwave heating to perform next cycle of staining. DAPI (WAS1301050, BioMed World) was used to stain nuclei and antifade mountant (WAS1302050, BioMed World) was applied. The primary antibody to CD56 (ab75813,

Abcam) and NKG2A (ab260035, Abcam) and second antibody (WAS1201100, BioMed World) were used. Image of immunofluorescence-stained slides were acquired with Nikon Eclipse Ci-L and 3DHISTECH Pannoramic MIDI II.

Flow cytometry

Lymphocytes were isolated from the whole blood using density gradient centrifugal method (P8610, Solarbio). Isolated cells were blocked (564219, BD Pharmingen) and stained with antibodies against CD3 (560835, BD Pharmingen), CD56 (555518, BD Pharmingen), NKG2A (375114, Biolegend), and TIGIT (568672, BD Pharmingen). For intracellular cytokine staining, cells were stimulated for 4 h with Leukocyte Activation Cocktail and BD GolgiPlug (550583, BD Pharmingen) according to manuals. After stimulation, cells were blocked, stained for surface markers, fixed and permeabilized with Fixation/Permeablization Kit (554714, BD Pharmingen). Fixed cells were stained with antibodies against IFNγ (552887, BD Pharmingen).

Construction and verification of prognostic model

On the basis of the markers of NK cell exhaustion, univariate Cox analysis was conducted in cholecystitis, pancreatitis, lung adenocarcinoma, and hepatocellular carcinoma patients to screen survival-related markers of NK cell exhaustion, and markers with P values < 0.05 were retained. We conducted multivariate analysis to identify the optimal prognostic markers for the prognostic model. The risk scores of the patients were calculated based on the normalized gene expression levels and the Cox regression coefficients of selected markers. Time-dependent receiver operating characteristic (ROC) curves were utilized to verify the prognostic performance of the model for overall survival (OS). For Kaplan-Meier survival, we used the R software package maxstat (Maximally selected rank statistics with multiple p-value approximations version: 0.7-25) to calculate the optimal cutoff value for RiskScore. We set the minimum group sample size to be greater than 25% and the maximum group sample size to be less than 75%, ultimately obtaining the optimal cutoff value. Based on this, patients were divided into high and low groups, and further analyzed the prognostic differences between the two groups using the R software

package's survival function. The logrank test method was used to evaluate the significance of prognostic differences between different groups of samples, and significant prognostic differences were ultimately observed.

Statistical analysis

Statistical analyses were performed using appropriate tests as indicated in legends (unpaired two-tailed t-test, chi-square test, and Wilcox test).

Data availability

sc-RNA sequening data that support the findings of this study have been deposited in Gene Expression Omnibus (GEO) with the accession numbers GSE254082.

Author contributions

Y.W., Q.F., H.W., and Q.Y. conceived the concept for this study. Y.J., J.X., L.J., and M.H. analyzed data and implemented experiments. C.D. conducted the bioinformatic analysis. L.J., Q.T., and Z.L. collected the clinical data and clinical samples. Y.J., J.X., and C.D. wrote the manuscript. W.Z. and Q. F. proofread the manuscript.

Fundings

This work was supported by grants from National Natural Science foundation of China (Project: 2021KY340; NSFC: 81773112 and 82073186 for Q.F.). This work was supported by Construction project of the State Administration of Traditional Chinese Medicine in 2021 (Teaching Letter [2021] No. 270 for Q.Y.). and Anhui Province Clinical Key Specialty Project in 2022 (Anhui Weichuan [2022] No. 297 for Q.Y.).

Competing interests

The authors declare no competing interests.

References

1 Elwood, D. R. Cholecystitis. *Surg Clin North Am* **88**, 1241-1252, viii (2008). https://doi.org:10.1016/j.suc.2008.07.008

2 Huffman, J. L. & Schenker, S. Acute acalculous cholecystitis: a review. *Clin Gastroenterol Hepatol* **8**, 15-22 (2010). https://doi.org:10.1016/j.cgh.2009.08.034

3 Markaki, I., Konsoula, A., Markaki, L., Spernovasilis, N. & Papadakis, M. Acute acalculous cholecystitis due to infectious causes. *World J Clin Cases* **9**, 6674-6685 (2021). https://doi.org:10.12998/wjcc.v9.i23.6674

4 Laurila, J. J. *et al.* Histopathology of acute acalculous cholecystitis in critically ill patients. *Histopathology* **47**, 485-492 (2005). https://doi.org:https://doi.org/10.1111/j.1365-2559.2005.02238.x

5 Fu, Y. T., Pang, L. W., Dai, W. L., Wu, S. D. & Kong, J. Advances in the Study of Acute Acalculous Cholecystitis: A Comprehensive Review. *Digest Dis* **40**, 468-478 (2022). https://doi.org:10.1159/000520025

6 Abu-Sbeih, H. *et al.* Case series of cancer patients who developed cholecystitis related to immune checkpoint inhibitor treatment. *J Immunother Cancer* **7** (2019). https://doi.org:ARTN 118 10.1186/s40425-019-0604-2

7 Loozen, C. S., Oor, J. E., van Ramshorst, B., van Santvoort, H. C. & Boerma, D. Conservative treatment of acute cholecystitis: a systematic review and pooled analysis. *Surg Endosc* **31**, 504-515 (2017). https://doi.org:10.1007/s00464-016-5011-x

527 8 van Dijk, A. H. *et al.* Systematic review of antibiotic treatment for acute calculous cholecystitis. *Brit J*
528 *Surg* **103**, 797-811 (2016). https://doi.org:10.1002/bjs.10146
529 9 Buonacera, A., Stancanelli, B., Colaci, M. & Malatino, L. Neutrophil to Lymphocyte Ratio: An
530 Emerging Marker of the Relationships between the Immune System and Diseases. *Int J Mol Sci* **23**
531 (2022). https://doi.org:10.3390/ijms23073636
532 10 McKinney, E. F. *et al.* A CD8+ T cell transcription signature predicts prognosis in autoimmune
533 disease. *Nat Med* **16**, 586-591, 581p following 591 (2010). https://doi.org:10.1038/nm.2130
534 11 McKinney, E. F., Lee, J. C., Jayne, D. R., Lyons, P. A. & Smith, K. G. T-cell exhaustion,
535 co-stimulation and clinical outcome in autoimmunity and infection. *Nature* **523**, 612-616 (2015).
536 https://doi.org:10.1038/nature14468
537 12 Sun, Y. *et al.* Single-cell landscape of the ecosystem in early-relapse hepatocellular carcinoma. *Cell*
538 **184**, 404-421 e416 (2021). https://doi.org:10.1016/j.cell.2020.11.041
539 13 Fridman, W. H., Zitvogel, L., Sautes-Fridman, C. & Kroemer, G. The immune contexture in cancer
540 prognosis and treatment. *Nat Rev Clin Oncol* **14**, 717-734 (2017).
541 https://doi.org:10.1038/nrclinonc.2017.101
542 14 Wouters, M. C. A. & Nelson, B. H. Prognostic Significance of Tumor-Infiltrating B Cells and Plasma
543 Cells in Human Cancer. *Clin Cancer Res* **24**, 6125-6135 (2018).
544 https://doi.org:10.1158/1078-0432.CCR-18-1481
545 15 Abel, A. M., Yang, C., Thakar, M. S. & Malarkannan, S. Natural Killer Cells: Development,
546 Maturation, and Clinical Utilization. *Front Immunol* **9**, 1869 (2018).

547 https://doi.org:10.3389/fimmu.2018.01869

548 16 Crinier, A., Narni-Mancinelli, E., Ugolini, S. & Vivier, E. SnapShot: Natural Killer Cells. *Cell* **180**,

549 1280-1280 e1281 (2020). https://doi.org:10.1016/j.cell.2020.02.029

550 17 Highton, A. J., Schuster, I. S., Degli-Esposti, M. A. & Altfeld, M. The role of natural killer cells in liver

551 inflammation. *Semin Immunopathol* **43**, 519-533 (2021).

552 https://doi.org:10.1007/s00281-021-00877-6

553 18 Parisi, L. *et al.* Natural Killer Cells in the Orchestration of Chronic Inflammatory Diseases. *J Immunol*

554 *Res* **2017**, 4218254 (2017). https://doi.org:10.1155/2017/4218254

555 19 Earls, R. H. & Lee, J. K. The role of natural killer cells in Parkinson's disease. *Exp Mol Med* **52**,

556 1517-1525 (2020). https://doi.org:10.1038/s12276-020-00505-7

557 20 Bi, J. & Tian, Z. NK Cell Exhaustion. *Front Immunol* **8**, 760 (2017).

558 https://doi.org:10.3389/fimmu.2017.00760

559 21 Zhang, Q. *et al.* Blockade of the checkpoint receptor TIGIT prevents NK cell exhaustion and elicits

560 potent anti-tumor immunity. *Nat Immunol* **19**, 723-732 (2018).

561 https://doi.org:10.1038/s41590-018-0132-0

562 22 Liu, X. *et al.* Immune checkpoint HLA-E:CD94-NKG2A mediates evasion of circulating tumor cells

563 from NK cell surveillance. *Cancer Cell* **41**, 272-287 e279 (2023).

564 https://doi.org:10.1016/j.ccell.2023.01.001

565 23 Zhang, C. *et al.* NKG2A is a NK cell exhaustion checkpoint for HCV persistence. *Nat Commun* **10**,

566 1507 (2019). https://doi.org:10.1038/s41467-019-09212-y

24 Sun, H. *et al.* Human CD96 Correlates to Natural Killer Cell Exhaustion and Predicts the Prognosis of Human Hepatocellular Carcinoma. *Hepatology* **70**, 168-183 (2019). https://doi.org:10.1002/hep.30347

25 Liu, G. *et al.* Increased TIGIT expressing NK cells with dysfunctional phenotype in AML patients correlated with poor prognosis. *Cancer Immunol Immunother* **71**, 277-287 (2022). https://doi.org:10.1007/s00262-021-02978-5

26 Sun, C. *et al.* High NKG2A expression contributes to NK cell exhaustion and predicts a poor prognosis of patients with liver cancer. *Oncoimmunology* **6**, e1264562 (2017). https://doi.org:10.1080/2162402X.2016.1264562

27 Crispe, I. N. The liver as a lymphoid organ. *Annu Rev Immunol* **27**, 147-163 (2009). https://doi.org:10.1146/annurev.immunol.021908.132629

28 Kubes, P. & Jenne, C. Immune Responses in the Liver. *Annu Rev Immunol* **36**, 247-277 (2018). https://doi.org:10.1146/annurev-immunol-051116-052415

29 Racanelli, V. & Rehermann, B. The liver as an immunological organ. *Hepatology* **43**, S54-62 (2006). https://doi.org:10.1002/hep.21060

30 Hardy, T., Oakley, F., Anstee, Q. M. & Day, C. P. Nonalcoholic Fatty Liver Disease: Pathogenesis and Disease Spectrum. *Annu Rev Pathol* **11**, 451-496 (2016). https://doi.org:10.1146/annurev-pathol-012615-044224

31 Armstrong, M. J., Adams, L. A., Canbay, A. & Syn, W. K. Extrahepatic complications of nonalcoholic fatty liver disease. *Hepatology* **59**, 1174-1197 (2014). https://doi.org:10.1002/hep.26717

587 32 Matyas, C., Haskó, G., Liaudet, L., Trojnar, E. & Pacher, P. Interplay of cardiovascular mediators,
588 oxidative stress and inflammation in liver disease and its complications. *Nature Reviews Cardiology*
589 **18**, 117-135 (2021). https://doi.org:10.1038/s41569-020-0433-5
590 33 Knab, L. M., Boller, A. M. & Mahvi, D. M. Cholecystitis. *Surg Clin North Am* **94**, 455-470 (2014).
591 https://doi.org:10.1016/j.suc.2014.01.005
592 34 Bandmann, O., Weiss, K. H. & Kaler, S. G. Wilson's disease and other neurological copper
593 disorders. *Lancet Neurol* **14**, 103-113 (2015). https://doi.org:10.1016/S1474-4422(14)70190-5
594 35 Huster, D. *et al.* Consequences of copper accumulation in the livers of the Atp7b-/- (Wilson disease
595 gene) knockout mice. *Am J Pathol* **168**, 423-434 (2006). https://doi.org:10.2353/ajpath.2006.050312
596 36 Medici, V. *et al.* Wilson's disease: changes in methionine metabolism and inflammation affect global
597 DNA methylation in early liver disease. *Hepatology* **57**, 555-565 (2013).
598 https://doi.org:10.1002/hep.26047
599 37 Huster, D. Structural and metabolic changes in Atp7b-/- mouse liver and potential for new
600 interventions in Wilson's disease. *Ann N Y Acad Sci* **1315**, 37-44 (2014).
601 https://doi.org:10.1111/nyas.12337
602 38 Aggarwal, A. & Bhatt, M. Wilson disease. *Curr Opin Neurol* **33**, 534-542 (2020).
603 https://doi.org:10.1097/WCO.0000000000000837
604 39 Cheng, N. *et al.* Spectrum of ATP7B mutations and genotype-phenotype correlation in large-scale
605 Chinese patients with Wilson Disease. *Clin Genet* **92**, 69-79 (2017).
606 https://doi.org:10.1111/cge.12951

607 40 Yang, G. M. *et al.* Prevalent Pathogenic Variants of ATP7B in Chinese Patients with Wilson's
608 Disease: Geographical Distribution and Founder Effect. *Genes (Basel)* **12** (2021).
609 https://doi.org:10.3390/genes12030336
610 41 Członkowska, A. *et al.* Wilson disease. *Nat Rev Dis Primers* **4**, 21 (2018).
611 https://doi.org:10.1038/s41572-018-0018-3
612 42 Roberts, E. A., Robinson, B. H. & Yang, S. Mitochondrial structure and function in the untreated
613 Jackson toxic milk (tx-j) mouse, a model for Wilson disease. *Mol Genet Metab* **93**, 54-65 (2008).
614 https://doi.org:10.1016/j.ymgme.2007.08.127
615 43 Zischka, H. & Lichtmannegger, J. Pathological mitochondrial copper overload in livers of Wilson's
616 disease patients and related animal models. *Ann N Y Acad Sci* **1315** (2014).
617 https://doi.org:10.1111/nyas.12347
618 44 Muchenditsi, A. *et al.* Systemic deletion of Atp7b modifies the hepatocytes' response to copper
619 overload in the mouse models of Wilson disease. *Sci Rep* **11**, 5659 (2021).
620 https://doi.org:10.1038/s41598-021-84894-3
621 45 He, S. *et al.* Single-cell transcriptome profiling of an adult human cell atlas of 15 major organs.
622 *Genome Biol* **21**, 294 (2020). https://doi.org:10.1186/s13059-020-02210-0
623 46 Sun, Y. *et al.* Single-cell landscape of the ecosystem in early-relapse hepatocellular carcinoma. *Cell*
624 **184** (2021). https://doi.org:10.1016/j.cell.2020.11.041
625 47 Li, Q. *et al.* Single-cell transcriptome profiling reveals vascular endothelial cell heterogeneity in
626 human skin. *Theranostics* **11**, 6461-6476 (2021). https://doi.org:10.7150/thno.54917

627 48 Sathe, A. *et al.* Single-Cell Genomic Characterization Reveals the Cellular Reprogramming of the
628 Gastric Tumor Microenvironment. *Clinical Cancer Research : an Official Journal of the American*
629 *Association For Cancer Research* **26**, 2640-2653 (2020).
630 https://doi.org:10.1158/1078-0432.CCR-19-3231
631 49 Wang, L. *et al.* Single-cell reconstruction of the adult human heart during heart failure and recovery
632 reveals the cellular landscape underlying cardiac function. *Nat Cell Biol* **22**, 108-119 (2020).
633 https://doi.org:10.1038/s41556-019-0446-7
634 50 Bhattacharjee, S. *et al.* Tumor restriction by type I collagen opposes tumor-promoting effects of
635 cancer-associated fibroblasts. *J Clin Invest* **131** (2021). https://doi.org:10.1172/JCI146987
636 51 Dumas, S. J. *et al.* Single-Cell RNA Sequencing Reveals Renal Endothelium Heterogeneity and
637 Metabolic Adaptation to Water Deprivation. *J Am Soc Nephrol* **31**, 118-138 (2020).
638 https://doi.org:10.1681/ASN.2019080832
639 52 Durante, M. A. *et al.* Single-cell analysis reveals new evolutionary complexity in uveal melanoma.
640 *Nature Communications* **11**, 496 (2020). https://doi.org:10.1038/s41467-019-14256-1
641 53 Gong, L. *et al.* Comprehensive single-cell sequencing reveals the stromal dynamics and
642 tumor-specific characteristics in the microenvironment of nasopharyngeal carcinoma. *Nature*
643 *Communications* **12**, 1540 (2021). https://doi.org:10.1038/s41467-021-21795-z
644 54 Wang, X. *et al.* Comparative analysis of cell lineage differentiation during hepatogenesis in humans
645 and mice at the single-cell transcriptome level. *Cell Res* **30**, 1109-1126 (2020).
646 https://doi.org:10.1038/s41422-020-0378-6

647 55 Zeng, Y. *et al.* Single-Cell RNA Sequencing Resolves Spatiotemporal Development of Pre-thymic
648 Lymphoid Progenitors and Thymus Organogenesis in Human Embryos. *Immunity* **51** (2019).
649 https://doi.org:10.1016/j.immuni.2019.09.008
650 56 Wu, F. *et al.* Single-cell profiling of tumor heterogeneity and the microenvironment in advanced
651 non-small cell lung cancer. *Nature Communications* **12**, 2540 (2021).
652 https://doi.org:10.1038/s41467-021-22801-0
653 57 Ramachandran, P. *et al.* Resolving the fibrotic niche of human liver cirrhosis at single-cell level.
654 *Nature* **575**, 512-518 (2019). https://doi.org:10.1038/s41586-019-1631-3
655 58 Pombo Antunes, A. R. *et al.* Single-cell profiling of myeloid cells in glioblastoma across species and
656 disease stage reveals macrophage competition and specialization. *Nat Neurosci* **24**, 595-610
657 (2021). https://doi.org:10.1038/s41593-020-00789-y
658 59 Strauss, O., Dunbar, P. R., Bartlett, A. & Phillips, A. The immunophenotype of antigen presenting
659 cells of the mononuclear phagocyte system in normal human liver--a systematic review. *J Hepatol*
660 **62**, 458-468 (2015). https://doi.org:10.1016/j.jhep.2014.10.006
661 60 Singh, M. *et al.* High-throughput targeted long-read single cell sequencing reveals the clonal and
662 transcriptional landscape of lymphocytes. *Nature Communications* **10**, 3120 (2019).
663 https://doi.org:10.1038/s41467-019-11049-4
664 61 Halbritter, F. *et al.* Epigenomics and Single-Cell Sequencing Define a Developmental Hierarchy in
665 Langerhans Cell Histiocytosis. *Cancer Discov* **9**, 1406-1421 (2019).
666 https://doi.org:10.1158/2159-8290.CD-19-0138

667 62 Bassez, A. *et al.* A single-cell map of intratumoral changes during anti-PD1 treatment of patients
668 with breast cancer. *Nature Medicine* **27**, 820-832 (2021).
669 https://doi.org:10.1038/s41591-021-01323-8
670 63 Popescu, D.-M. *et al.* Decoding human fetal liver haematopoiesis. *Nature* **574**, 365-371 (2019).
671 https://doi.org:10.1038/s41586-019-1652-y
672 64 Chen, Y.-P. *et al.* Single-cell transcriptomics reveals regulators underlying immune cell diversity and
673 immune subtypes associated with prognosis in nasopharyngeal carcinoma. *Cell Res* **30**, 1024-1042
674 (2020). https://doi.org:10.1038/s41422-020-0374-x
675 65 Wang, J. *et al.* Liver Immune Profiling Reveals Pathogenesis and Therapeutics for Biliary Atresia.
676 *Cell* **183** (2020). https://doi.org:10.1016/j.cell.2020.10.048
677 66 Dixon, L. J., Barnes, M., Tang, H., Pritchard, M. T. & Nagy, L. E. Kupffer cells in the liver. *Compr*
678 *Physiol* **3**, 785-797 (2013). https://doi.org:10.1002/cphy.c120026
679 67 Cella, M. *et al.* Subsets of ILC3-ILC1-like cells generate a diversity spectrum of innate lymphoid
680 cells in human mucosal tissues. *Nature Immunology* **20**, 980-991 (2019).
681 https://doi.org:10.1038/s41590-019-0425-y
682 68 Elmentaite, R. *et al.* Cells of the human intestinal tract mapped across space and time. *Nature* **597**,
683 250-255 (2021). https://doi.org:10.1038/s41586-021-03852-1
684 69 Liu, Y. *et al.* Single-cell analysis reveals immune landscape in kidneys of patients with chronic
685 transplant rejection. *Theranostics* **10**, 8851-8862 (2020). https://doi.org:10.7150/thno.48201
686 70 Wang, L. *et al.* Nanoparticle enhanced combination therapy for stem-like progenitors defined by

single-cell transcriptomics in chemotherapy-resistant osteosarcoma. *Signal Transduction and Targeted Therapy* **5**, 196 (2020). https://doi.org:10.1038/s41392-020-00248-x

71 Tirosh, I. *et al.* Dissecting the multicellular ecosystem of metastatic melanoma by single-cell RNA-seq. *Science (New York, N.Y.)* **352**, 189-196 (2016). https://doi.org:10.1126/science.aad0501

72 Jaeger, N. *et al.* Single-cell analyses of Crohn's disease tissues reveal intestinal intraepithelial T cells heterogeneity and altered subset distributions. *Nature Communications* **12**, 1921 (2021). https://doi.org:10.1038/s41467-021-22164-6

73 Depuydt, M. A. C. *et al.* Microanatomy of the Human Atherosclerotic Plaque by Single-Cell Transcriptomics. *Circ Res* **127**, 1437-1455 (2020). https://doi.org:10.1161/CIRCRESAHA.120.316770

74 Andor, N. *et al.* Single-cell RNA-Seq of follicular lymphoma reveals malignant B-cell types and coexpression of T-cell immune checkpoints. *Blood* **133**, 1119-1129 (2019). https://doi.org:10.1182/blood-2018-08-862292

75 Heming, M. *et al.* Neurological Manifestations of COVID-19 Feature T Cell Exhaustion and Dedifferentiated Monocytes in Cerebrospinal Fluid. *Immunity* **54** (2021). https://doi.org:10.1016/j.immuni.2020.12.011

76 Xin, Z. *et al.* The immune landscape of human thymic epithelial tumors. *Nature Communications* **13**, 5463 (2022). https://doi.org:10.1038/s41467-022-33170-7

77 Zhao, J. *et al.* Single-cell RNA sequencing reveals the heterogeneity of liver-resident immune cells in human. *Cell Discovery* **6**, 22 (2020). https://doi.org:10.1038/s41421-020-0157-z

707 78 Williams, D. W. *et al.* Human oral mucosa cell atlas reveals a stromal-neutrophil axis regulating
708 tissue immunity. *Cell* **184** (2021). https://doi.org:10.1016/j.cell.2021.05.013
709 79 Madissoon, E. *et al.* scRNA-seq assessment of the human lung, spleen, and esophagus tissue
710 stability after cold preservation. *Genome Biol* **21**, 1 (2019).
711 https://doi.org:10.1186/s13059-019-1906-x
712 80 Zhang, F. *et al.* Adaptive immune responses to SARS-CoV-2 infection in severe versus mild
713 individuals. *Signal Transduction and Targeted Therapy* **5**, 156 (2020).
714 https://doi.org:10.1038/s41392-020-00263-y
715 81 Fernandez, D. M. *et al.* Single-cell immune landscape of human atherosclerotic plaques. *Nature*
716 *Medicine* **25**, 1576-1588 (2019). https://doi.org:10.1038/s41591-019-0590-4
717 82 Luoma, A. M. *et al.* Molecular Pathways of Colon Inflammation Induced by Cancer Immunotherapy.
718 *Cell* **182** (2020). https://doi.org:10.1016/j.cell.2020.06.001
719 83 Zhang, X. *et al.* Persistence of cirrhosis is maintained by intrahepatic regulatory T cells that inhibit
720 fibrosis resolution by regulating the balance of tissue inhibitors of metalloproteinases and matrix
721 metalloproteinases. *Transl Res* **169**, 67-79 e61-62 (2016). https://doi.org:10.1016/j.trsl.2015.10.008
722 84 Shevtsov, M. & Multhoff, G. Heat Shock Protein-Peptide and HSP-Based Immunotherapies for the
723 Treatment of Cancer. *Front Immunol* **7**, 171 (2016). https://doi.org:10.3389/fimmu.2016.00171
724 85 Zhang, Q. *et al.* Landscape and Dynamics of Single Immune Cells in Hepatocellular Carcinoma.
725 *Cell* **179**, 829-845 e820 (2019). https://doi.org:10.1016/j.cell.2019.10.003
726 86 Wang, X. *et al.* Single-cell dissection of remodeled inflammatory ecosystem in primary and

727 metastatic gallbladder carcinoma. *Cell Discov* **8**, 101 (2022).
728 https://doi.org:10.1038/s41421-022-00445-8
729 87 Tang, J., Yan, Z., Feng, Q., Yu, L. & Wang, H. The Roles of Neutrophils in the Pathogenesis of Liver
730 Diseases. *Front Immunol* **12**, 625472 (2021). https://doi.org:10.3389/fimmu.2021.625472
731 88 Cho, Y. & Szabo, G. Two Faces of Neutrophils in Liver Disease Development and Progression.
732 *Hepatology* **74**, 503-512 (2021). https://doi.org:10.1002/hep.31680
733 89 Wang, S. *et al.* S100A8/A9 in Inflammation. *Front Immunol* **9**, 1298 (2018).
734 https://doi.org:10.3389/fimmu.2018.01298
735 90 Chen, Y., Ouyang, Y., Li, Z., Wang, X. & Ma, J. S100A8 and S100A9 in Cancer. *Biochim Biophys*
736 *Acta Rev Cancer* **1878**, 188891 (2023). https://doi.org:10.1016/j.bbcan.2023.188891
737 91 André, P. *et al.* Anti-NKG2A mAb Is a Checkpoint Inhibitor that Promotes Anti-tumor Immunity by
738 Unleashing Both T and NK Cells. *Cell* **175**, 1731-+ (2018). https://doi.org:10.1016/j.cell.2018.10.014
739 92 Brillantes, M. & Beaulieu, A. M. Transcriptional control of natural killer cell differentiation.
740 *Immunology* **156**, 111-119 (2019). https://doi.org:10.1111/imm.13017
741 93 Zhang, J., Rousseaux, N. & Walzer, T. Eomes and T-bet, a dynamic duo regulating NK cell
742 differentiation. *Bioessays* **44**, e2100281 (2022). https://doi.org:10.1002/bies.202100281
743 94 da Silva, I. P. *et al.* Reversal of NK-cell exhaustion in advanced melanoma by Tim-3 blockade.
744 *Cancer Immunol Res* **2**, 410-422 (2014). https://doi.org:10.1158/2326-6066.CIR-13-0171
745 95 Sun, C., Sun, H., Zhang, C. & Tian, Z. NK cell receptor imbalance and NK cell dysfunction in HBV
746 infection and hepatocellular carcinoma. *Cell Mol Immunol* **12**, 292-302 (2015).

https://doi.org:10.1038/cmi.2014.91

96 Hosseini, R. *et al.* Cancer exosomes and natural killer cells dysfunction: biological roles, clinical significance and implications for immunotherapy. *Molecular Cancer* **21** (2022). https://doi.org:ARTN 15 10.1186/s12943-021-01492-7

97 Park, J., Hsueh, P. C., Li, Z. Y. & Ho, P. C. Microenvironment-driven metabolic adaptations guiding CD8+T cell anti-tumor immunity. *Immunity* **56**, 32-42 (2023). https://doi.org:10.1016/j.immuni.2022.12.008

98 Yan, C. S. *et al.* Exhaustion-associated cholesterol deficiency dampens the cytotoxic arm of antitumor immunity. *Cancer Cell* **41**, 1276-+ (2023). https://doi.org:10.1016/j.ccell.2023.04.016

99 Bader, J. E., Voss, K. & Rathmell, J. C. Targeting Metabolism to Improve the Tumor Microenvironment for Cancer Immunotherapy. *Mol Cell* **78**, 1019-1033 (2020). https://doi.org:10.1016/j.molcel.2020.05.034

100 Riera-Domingo, C. *et al.* Immunity, Hypoxia, and Metabolism-the Menage a Trois of Cancer: Implications for Immunotherapy. *Physiol Rev* **100**, 1-102 (2020). https://doi.org:10.1152/physrev.00018.2019

101 Wu, S. Y., Fu, T., Jiang, Y. Z. & Shao, Z. M. Natural killer cells in cancer biology and therapy. *Molecular Cancer* **19** (2020). https://doi.org:ARTN 120 10.1186/s12943-020-01238-x

102 Poznanski, S. M. & Ashkar, A. A. What Defines NK Cell Functional Fate: Phenotype or Metabolism?

Frontiers in Immunology **10** (2019). https://doi.org:ARTN 1414
10.3389/fimmu.2019.01414

103 O'Brien, K. L. & Finlay, D. K. Immunometabolism and natural killer cell responses. *Nat Rev Immunol* **19**, 282-290 (2019). https://doi.org:10.1038/s41577-019-0139-2

104 Tsvetkov, P. *et al.* Copper induces cell death by targeting lipoylated TCA cycle proteins. *Science* **375**, 1254-+ (2022). https://doi.org:10.1126/science.abf0529

105 Yu, G. C., Wang, L. G., Han, Y. Y. & He, Q. Y. clusterProfiler: an R Package for Comparing Biological Themes Among Gene Clusters. *Omics* **16**, 284-287 (2012). https://doi.org:10.1089/omi.2011.0118

106 Jin, S. Q. *et al.* Inference and analysis of cell-cell communication using CellChat. *Nature Communications* **12** (2021). https://doi.org:ARTN 1088
10.1038/s41467-021-21246-9

107 Qiu, X. J. *et al.* Single-cell mRNA quantification and differential analysis with Census. *Nat Methods* **14**, 309-+ (2017). https://doi.org:10.1038/Nmeth.4150

108 Gulati, G. S. *et al.* Single-cell transcriptional diversity is a hallmark of developmental potential. *Science* **367**, 405-+ (2020). https://doi.org:10.1126/science.aax0249

109 van de Sande, B. *et al.* A scalable SCENIC workflow for single-cell gene regulatory network analysis. *Nat Protoc* **15**, 2247-2276 (2020). https://doi.org:10.1038/s41596-020-0336-2

110 Andreatta, M. & Carmona, S. J. UCell: Robust and scalable single-cell gene signature scoring. *Comput Struct Biotec* **19**, 3796-3798 (2021). https://doi.org:10.1016/j.csbj.2021.06.043

Figure 1

a.

Genotypes of ATP7B in 20 WD cases

Mutant alleles*	Amino acid change	No. (%)
c.2333G>T	p.R778L	13 (65%)
c.2804C>T	p.T935M	0 (0%)
c.2975C>T	p.P992L	0 (0%)
Unknow	Unknow	7 (35%)

* Reference. Seq: NM_000053.4

b.

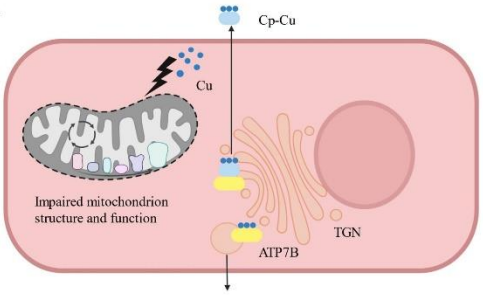

c.

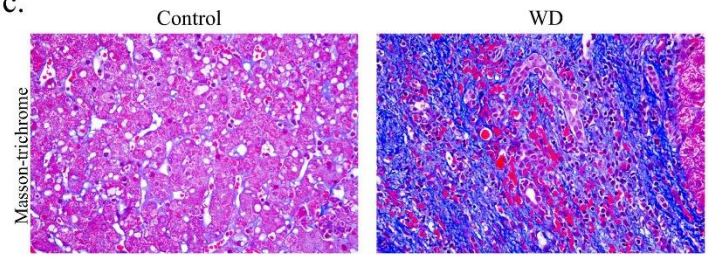

d.

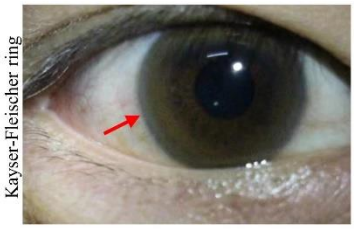

e.

Clinical statistics of the patients.

Cohort 1			
	WD (n=92)	HBV (n=95)	*P* value
TBIL - μmol/L (≤26)	14.90±6.59	20.46±13.94	0.0007
TG - μmol/L (≤1.7)	0.98±0.58	0.99±0.71	0.7699
T-CHOL - μmol/L (3-5.7)	4.09±0.75	3.84±1.13	0.0743

Cohort 2			
	WD (n=618)	HBV (n=370)	*P* value
Hyperglycemia – no. (%)	33 (5.34%)	42 (11.35%)	0.0006
Gallstone – no. (%)	65 (10.52%)	39 (10.54%)	0.9910
Cholecystitis – no. (%)	306 (49.51%)	35 (9.46%)	0.0001

Cohort 3			
	Cholecystitis & WD (n=34)	Cholecystitis (n=44)	*P* value
WBC – no. (%)	12 (35.29%)	1 (2.27%)	0.0004
NEU – no. (%)	10 (29.41%)	5 (11.36%)	0.0449
LYM – no. (%)	11 (32.35%)	6 (13.64%)	0.0471
TBIL – no. (%)	5 (14.71%)	6 (13.64%)	0.8929
ALB – no. (%)	10 (29.41%)	10 (22.73%)	0.5026
ALT – no. (%)	18 (52.94%)	28 (63.64%)	0.3410
AST – no. (%)	9 (26.47%)	11 (25.00%)	0.8827

WD, Wilson disease; HBV, Hepatitis B virus; ; TBIL, Total bilirubin; TG, Triglyceride; T-CHOL, Total cholesterol; WBC, White blood cell; NEU, Neutrophil; LYM, Lymphocyte; ALB, Albumin; ALT, Alanine aminotransferase; AST, Aspartate aminotransferase.

Figure 1. Clinical manifestation of WD patients and WD causes poor prognosis of cholecystitis. **a.** DNA sequencing result of 20 WD patients was summarized in the graph. **b.** The schematic diagram illustrates copper transport disturbances caused by ATP7B mutations, along with structural and functional impairments in mitochondria. Created with BioRender.com. **c.** Masson-trichrome staining of liver tissues of patients with WD and control. **d.** The picture of Kayser-Fleischer (KF) ring in the cornea of a patient with WD, captured during clinical examination. **e.** The table of clinical statistics of patients in 3 cohorts. Data are mean± S.D. Unpaired two-tailed t-test and chi-square test.

Figure 2

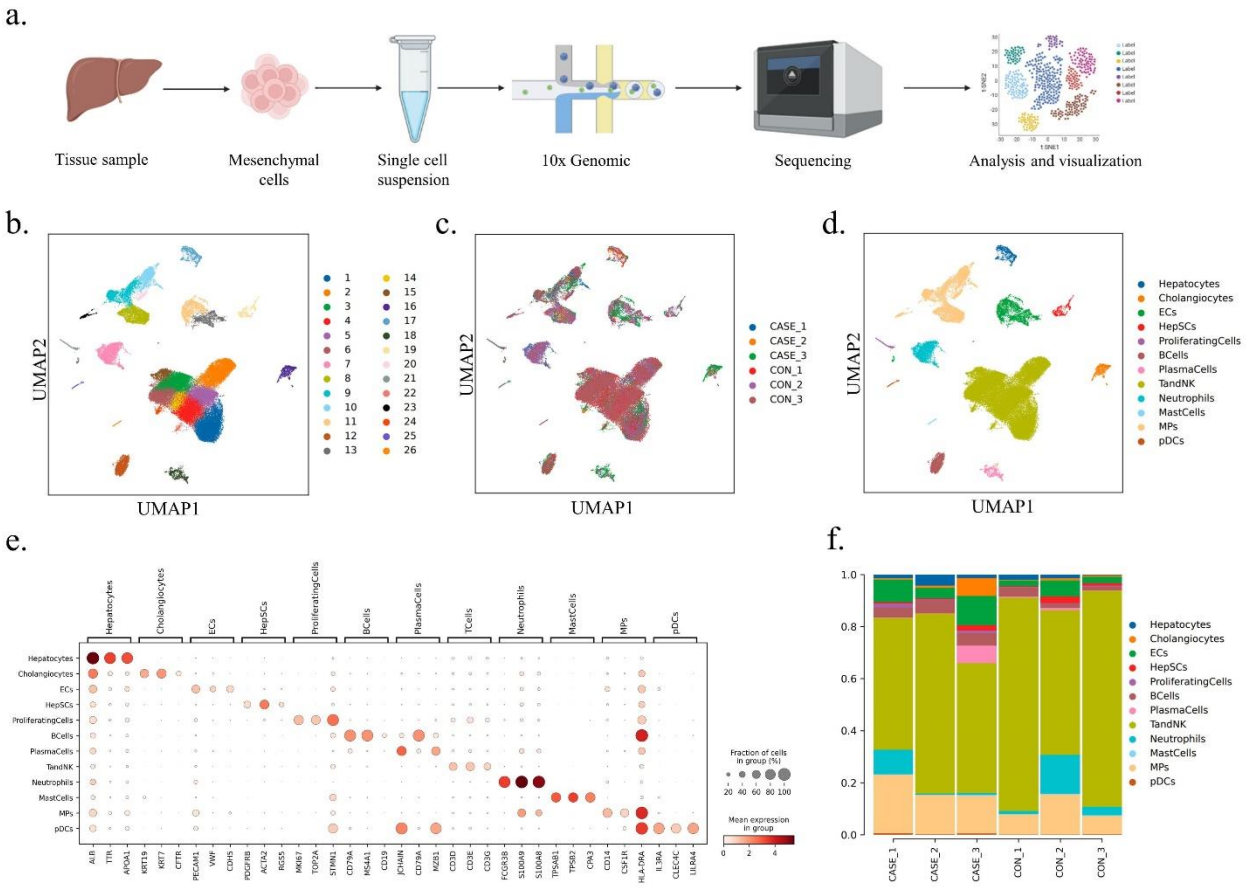
a.
Tissue sample
Mesenchymal cells
Single cell suspension
10x Genomic
Sequencing
Analysis and visualization
b.
UMAP2
UMAP1
c.
CASE_1
CASE_2
CASE_3
CON_1
CON_2
CON_3
d.
Hepatocytes
Cholangiocytes
ECs
HepSCs
ProliferatingCells
BCells
PlasmaCells
TandNK
Neutrophils
MastCells
MPs
pDCs
e.
Fraction of cells in group (%)
Mean expression in group
f.

Figure 2. Single-cell profiling of non-parenchymal cells in the liver of WD patients. **a.** The workflow of scRNA-seq. Created with BioRender.com. **b.** UMAP visualization of 26 principal components of all the single cells. **c.** UMAP visualization of 26 principal components by samples. **d.** UMAP visualization of 12 main cell types. **e.** The dot plot showing the expression of top 3 marker genes in 12 main cell types.

Figure 3

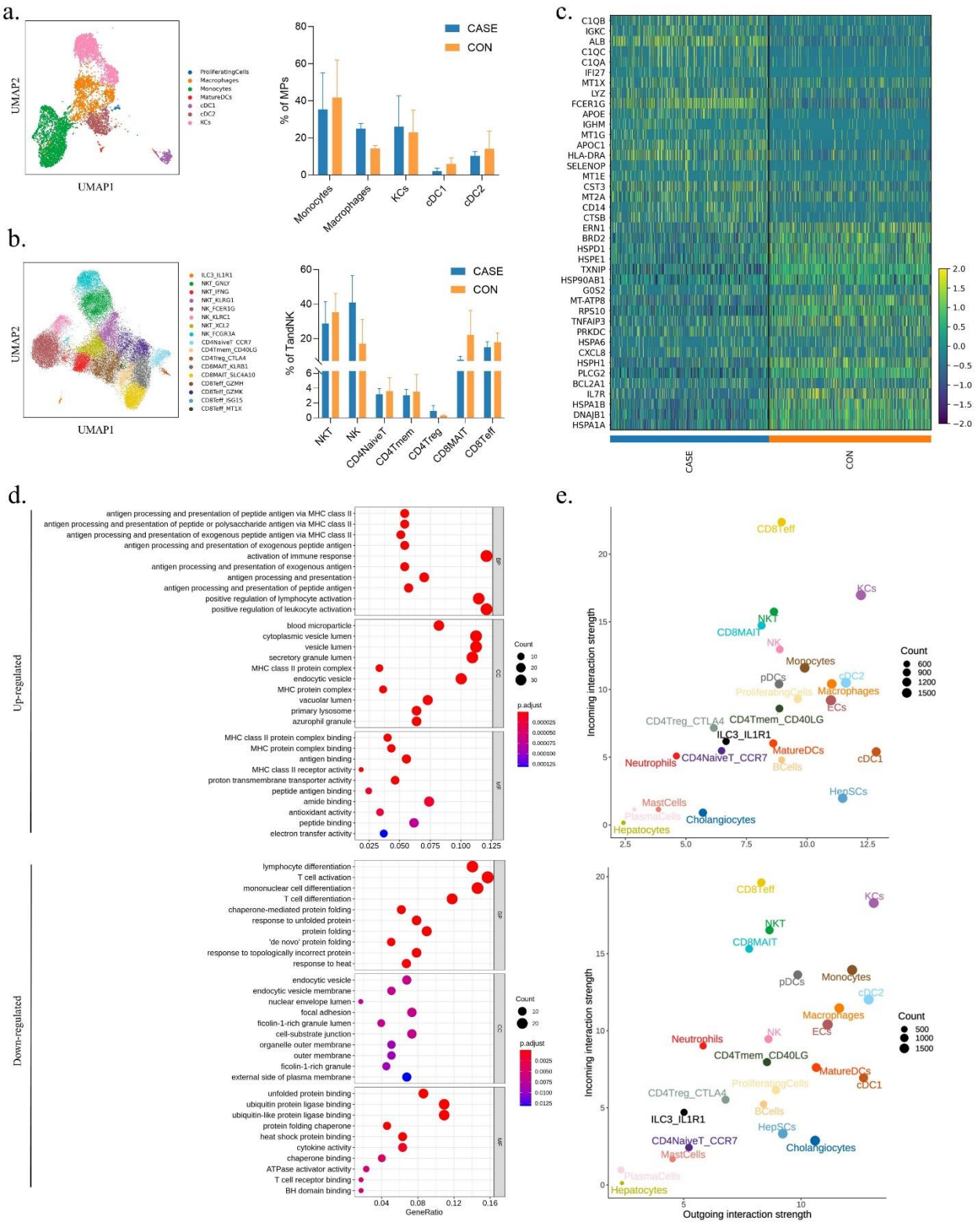
a.
UMAP2
UMAP1
ProliferatingCells
Macrophages
Monocytes
MatureDCs
cDC1
cDC2
KCs
% of MPs
CASE
CON
Monocytes
Macrophages
KCs
cDC1
cDC2
b.
ILC3_IL1R1
NKT_GNLY
NKT_IFNG
NKT_KLRG1
NK_FCER1G
NK_KLRC1
NKT_XCL2
NK_FCGR3A
CD4NaiveT_CCR7
CD4Tmem_CD40LG
CD4Treg_CTLA4
CD8MAIT_KLRB1
CD8MAIT_SLC4A10
CD8Teff_GZMH
CD8Teff_GZMK
CD8Teff_ISG15
CD8Teff_MT1X
% of TandNK
NKT
NK
CD4NaiveT
CD4Tmem
CD4Treg
CD8MAIT
CD8Teff
c.
C1QB
IGKC
ALB
C1QC
C1QA
IFI27
MT1X
LYZ
FCER1G
APOE
IGHM
MT1G
APOC1
HLA-DRA
SELENOP
MT1E
CST3
MT2A
CD14
CTSB
ERN1
BRD2
HSPD1
HSPE1
TXNIP
HSP90AB1
G0S2
MT-ATP8
RPS10
TNFAIP3
PRKDC
HSPA6
CXCL8
HSPH1
PLCG2
BCL2A1
IL7R
HSPA1B
DNAJB1
HSPA1A
CASE
CON
d.
Up-regulated
antigen processing and presentation of peptide antigen via MHC class II
antigen processing and presentation of peptide or polysaccharide antigen via MHC class II
antigen processing and presentation of exogenous peptide antigen via MHC class II
antigen processing and presentation of exogenous peptide antigen
activation of immune response
antigen processing and presentation of exogenous antigen
antigen processing and presentation
antigen processing and presentation of peptide antigen
positive regulation of lymphocyte activation
positive regulation of leukocyte activation
BP
blood microparticle
cytoplasmic vesicle lumen
vesicle lumen
secretory granule lumen
MHC class II protein complex
endocytic vesicle
MHC protein complex
vacuolar lumen
primary lysosome
azurophil granule
CC
MHC class II protein complex binding
MHC protein complex binding
antigen binding
MHC class II receptor activity
proton transmembrane transporter activity
peptide antigen binding
amide binding
antioxidant activity
peptide binding
electron transfer activity
MF
Count
p.adjust
Down-regulated
lymphocyte differentiation
T cell activation
mononuclear cell differentiation
T cell differentiation
chaperone-mediated protein folding
response to unfolded protein
protein folding
'de novo' protein folding
response to topologically incorrect protein
response to heat
BP
endocytic vesicle
endocytic vesicle membrane
nuclear envelope lumen
focal adhesion
ficolin-1-rich granule lumen
cell-substrate junction
organelle outer membrane
outer membrane
ficolin-1-rich granule
external side of plasma membrane
CC
unfolded protein binding
ubiquitin protein ligase binding
ubiquitin-like protein ligase binding
protein folding chaperone
heat shock protein binding
cytokine activity
chaperone binding
ATPase activator activity
T cell receptor binding
BH domain binding
MF
GeneRatio
e.
Incoming interaction strength
Outgoing interaction strength
CD8Teff
KCs
NKT
CD8MAIT
NK
Monocytes
pDCs
cDC2
ProliferatingCells
Macrophages
ECs
CD4Treg_CTLA4
CD4Tmem_CD40LG
ILC3_IL1R1
MatureDCs
Neutrophils
CD4NaiveT_CCR7
BCells
cDC1
HepSCs
MastCells
PlasmaCells
Cholangiocytes
Hepatocytes
Count

Figure 3. The altered immune microenvironment in WD patients. **a.** UMAP visualization of MPs colored and labeled by cell subtypes (left). The bar chart showing the average percentage of different subtypes in case group (n=3) and control group (n=3) (right). Data are mean ± S.D. **b.** UMAP visualization of T and NK cells colored and labeled by cell subtypes (left). The bar chart showing the average percentage of different subtypes in case group (n=3) and control group (n=3) (right). Data are mean± S.D. **c.** The heatmap showing the top 20 differently expressed genes (DEGs) for all immune cells. **d.** The dot plot showing GO enrichment on DEGs of all immune cells between the case and control group. BP, biological processes; CC, cellular components; MF, molecular function. **e.** The scatter showing the strength of all cell subtypes in signal incoming and outgoing. Upper, the case group; down, the control group.

Figure 4

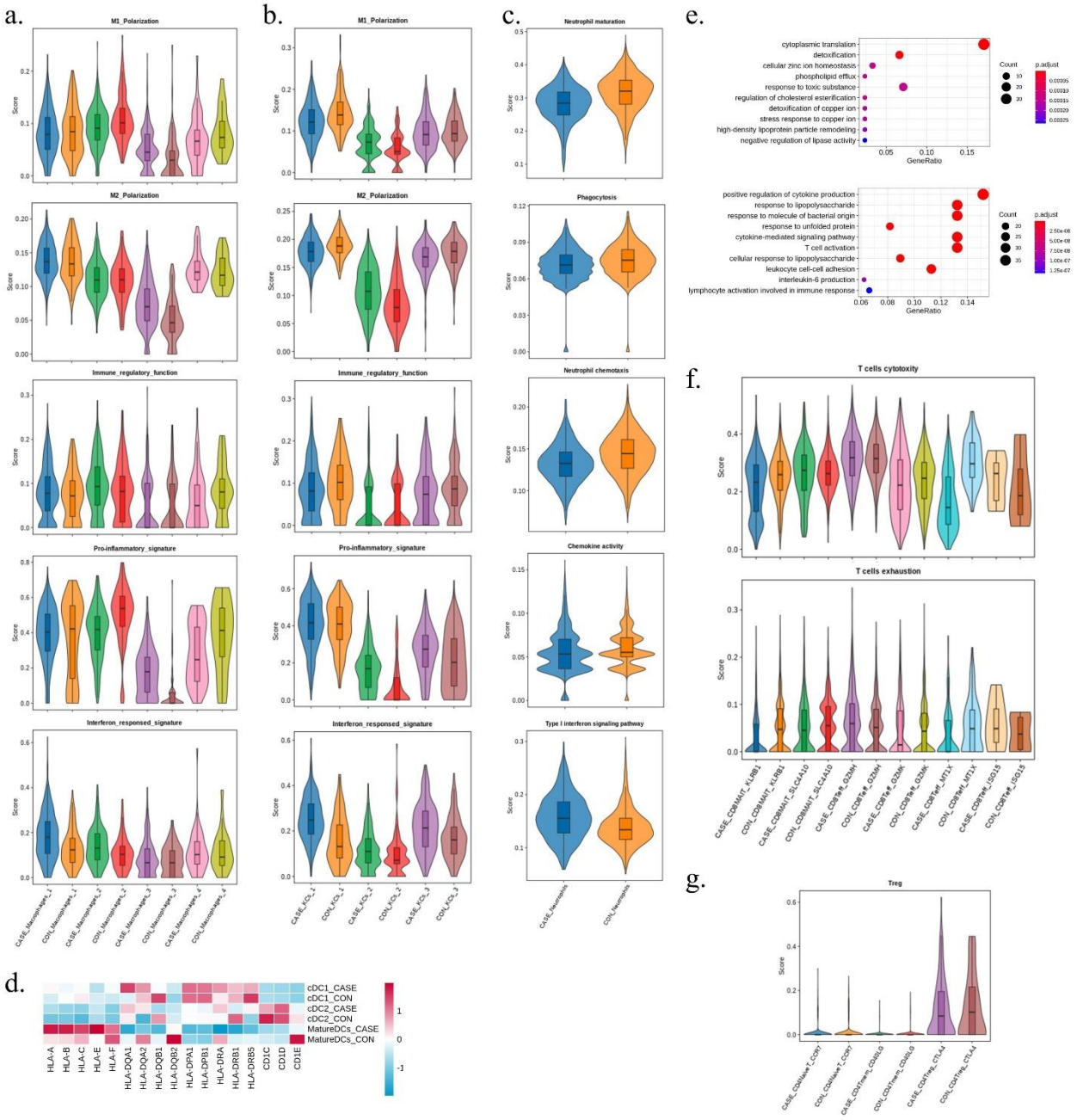
a.
M1_Polarization
M2_Polarization
Immune_regulatory_function
Pro-inflammatory_signature
Interferon_responsed_signature
Score
CASE_Neutrophils_1
CON_Neutrophils_1
CASE_Neutrophils_2
CON_Neutrophils_2
CASE_Neutrophils_3
CON_Neutrophils_3
CASE_Neutrophils_4
CON_Neutrophils_4
b.
M1_Polarization
M2_Polarization
Immune_regulatory_function
Pro-inflammatory_signature
Interferon_responsed_signature
CASE_KCS_1
CON_KCS_1
CASE_KCS_2
CON_KCS_2
CASE_KCS_3
CON_KCS_3
c.
Neutrophil maturation
Phagocytosis
Neutrophil chemotaxis
Chemokine activity
Type I interferon signaling pathway
CASE_Neutrophils
CON_Neutrophils
e.
cytoplasmic translation
detoxification
cellular zinc ion homeostasis
phospholipid efflux
response to toxic substance
regulation of cholesterol esterification
detoxification of copper ion
stress response to copper ion
high-density lipoprotein particle remodeling
negative regulation of lipase activity
GeneRatio
Count
p.adjust
positive regulation of cytokine production
response to lipopolysaccharide
response to molecule of bacterial origin
response to unfolded protein
cytokine-mediated signaling pathway
T cell activation
cellular response to lipopolysaccharide
leukocyte cell-cell adhesion
interleukin-6 production
lymphocyte activation involved in immune response
f.
T cells cytotoxity
T cells exhaustion
CASE_CD8MAIT_KLRB1
CON_CD8MAIT_KLRB1
CASE_CD8MAIT_SLC4A10
CON_CD8MAIT_SLC4A10
CASE_CD8Tem_GZMH
CON_CD8Tem_GZMH
CASE_CD8Tem_GZMK
CON_CD8Tem_GZMK
CASE_CD8Tef_MTIX
CON_CD8Tef_MTIX
CASE_CD8Tef_ISG15
CON_CD8Tef_ISG15
g.
Treg
CASE_CD4Naive_CCR7
CON_CD4Naive_CCR7
CASE_CD4Tmem_CD40LG
CON_CD4Tmem_CD40LG
CASE_CD4Treg_CTLA4
CON_CD4Treg_CTLA4
d.
cDC1_CASE
cDC1_CON
cDC2_CASE
cDC2_CON
MatureDCs_CASE
MatureDCs_CON
HLA-A
HLA-B
HLA-C
HLA-E
HLA-F
HLA-DQA1
HLA-DQA2
HLA-DQB1
HLA-DQB2
HLA-DPA1
HLA-DPB1
HLA-DRA
HLA-DRB1
HLA-DRB5
CD1C
CD1D
CD1E

Figure 4. The dysfunction of main immune cells in WD patients. **a.** The violin plots displaying M1 polarization, M2 polarization, pro-inflammatory signature, and interferon responsed signature of the 4 subtypes within macrophages between two groups by gene scoring. **b.** The violin plots displaying M1 polarization, M2 polarization, pro-inflammatory signature, and interferon responsed signature of the 3 subtypes within Kupffer cells between two groups by gene scoring. **c.** The violin plots displaying maturation, phagocytosis, chemotaxis, chemokine activity and Type I interferon signaling pathway scores within neutrophils between two groups. **d.** The heatmap showing the relative expression level of genes in each cell subtype between the case and control group. **e.** The dot plot showing biological process of GO enrichment on differentially expressed genes (DEGs) in monocytes between the case and control group. Upper, upregulation; down, downregulation. **f.** The violin plots displaying cytotoxicity and exhaustion scores of the 6 cell subtypes within CD8 T cells between two groups by gene scoring. **g.** The violin plots displaying Treg scores of the 3 cell subtypes within CD4 T cells between two groups by gene scoring.

Figure 5

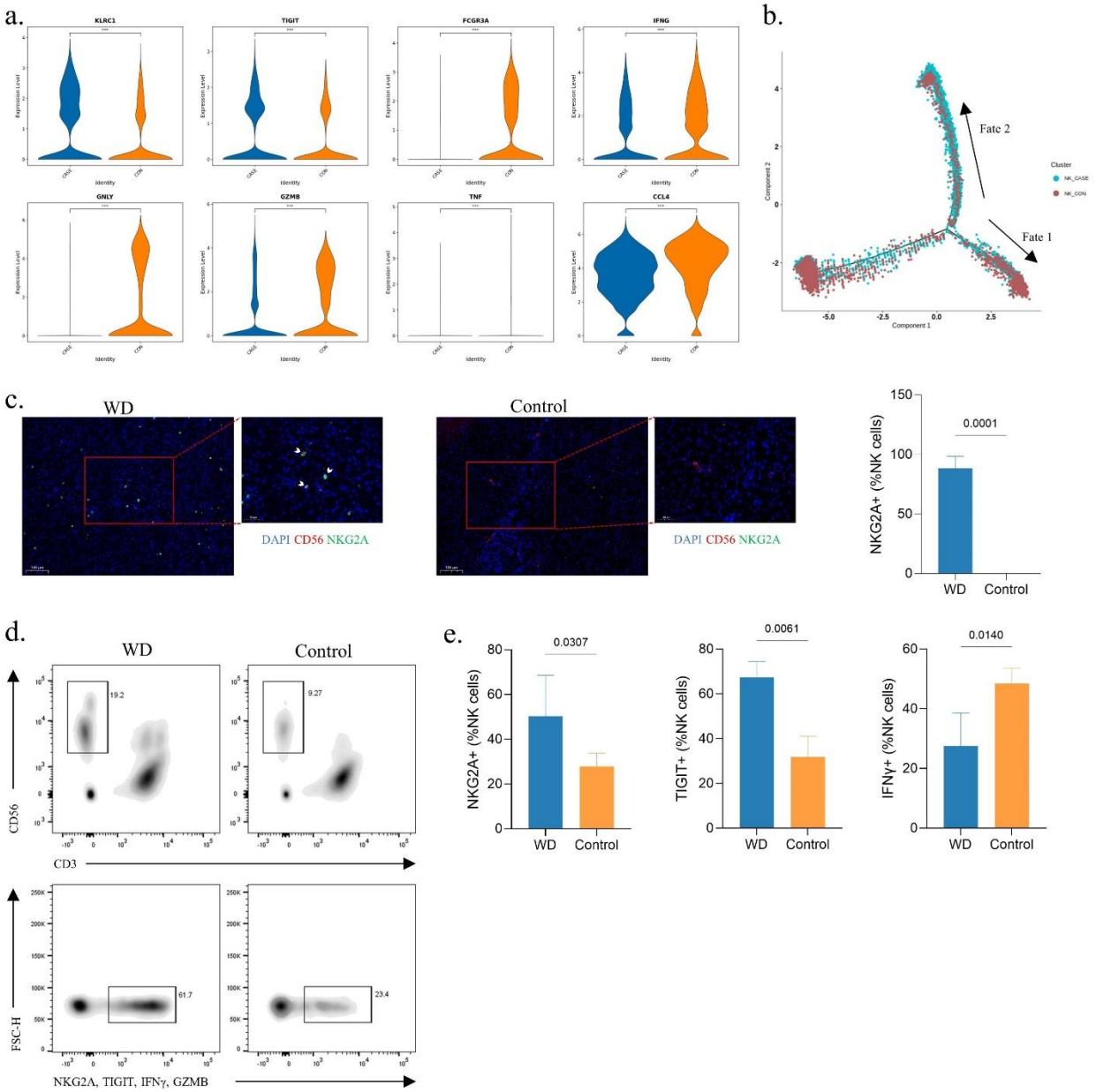
a.
KLRC1
TIGIT
FCGR3A
IFNG
GNLY
GZMB
TNF
CCL4
Expression Level
Identity
CASE
CON
b.
Fate 2
Fate 1
Cluster
NK_CASE
NK_CON
Component 1
Component 2
c.
WD
Control
DAPI CD56 NKG2A
NKG2A+ (%NK cells)
0.0001
d.
WD
Control
CD56
CD3
19.2
9.27
FSC-H
NKG2A, TIGIT, IFNγ, GZMB
61.7
23.4
e.
NKG2A+ (%NK cells)
0.0307
TIGIT+ (%NK cells)
0.0061
IFNγ+ (%NK cells)
0.0140

Figure 5. Identification of NK cell exhaustion in WD patients. **a.** The violin plots showing the relative expression level of genes in NK cells between the case and control group. ***, $P<0.001$; Wilcox test. **b.** Trajectories of NK cells in the case and control group. **c.** Representative immunofluorescence staining for NK cells (CD56) and expression of NKG2A in liver tissues of WD and control. Scale bars, 100 μm for 40X and 50 μm for 100X. $NKG2A^+$ NK cells are highlighted by arrows. Quantifications were performed by assessing three random fields per slide. Data are mean± S.D. Unpaired two-tailed t-test. **d.** Gating strategy applied in flow cytometry. **e.** The bar charts showing the percentage of $NKG2A^+$ (WD, n=5; Control, n=5), $TIGIT^+$ (WD, n=3; Control, n=3), and $IFN\gamma^+$ (WD, n=4; Control, n=4) NK cells. Data are mean± S.D. Unpaired two-tailed t-test.

Figure 6

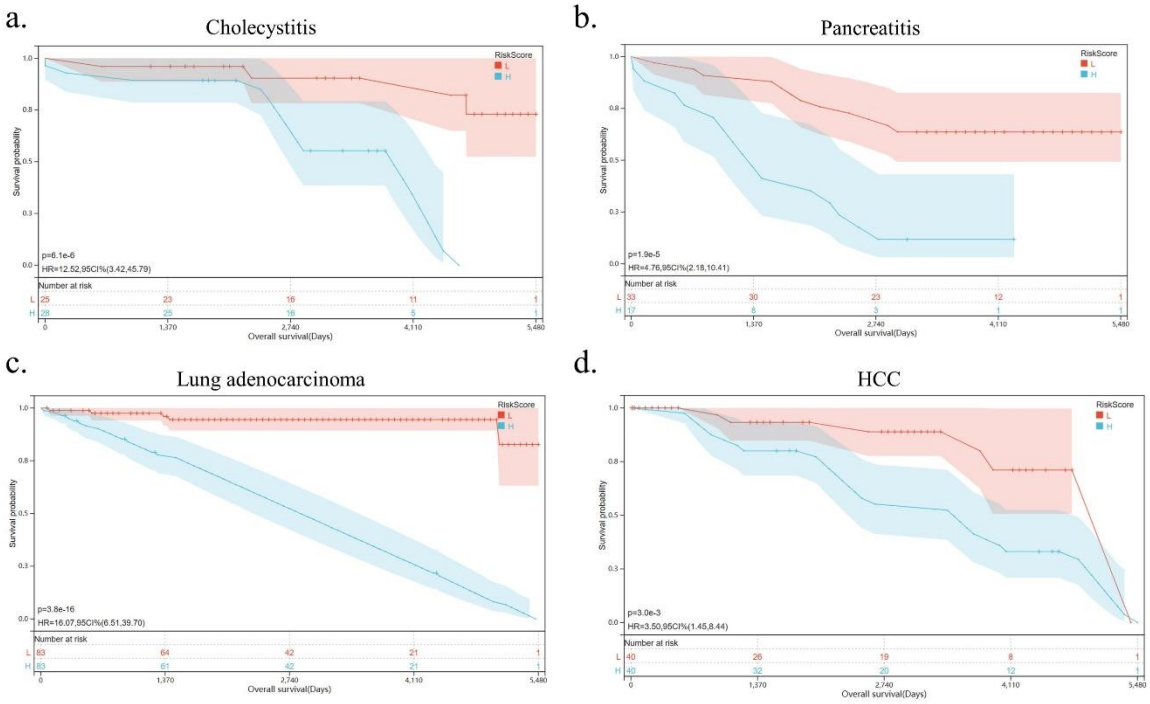
a.
Cholecystitis
RiskScore
L
H
Survival probability
p=6.1e-6
HR=12.52,95CI%(3.42,45.79)
Number at risk
L 25 23 16 11 1
H 28 25 16 5 1
0 1,370 2,740 4,110 5,480
Overall survival(Days)
b.
Pancreatitis
RiskScore
L
H
Survival probability
p=1.9e-5
HR=4.76,95CI%(2.18,10.41)
Number at risk
L 33 30 23 12 1
H 17 8 5 1 1
0 1,370 2,740 4,110 5,480
Overall survival(Days)
c.
Lung adenocarcinoma
RiskScore
L
H
Survival probability
p=3.8e-16
HR=16.07,95CI%(6.51,39.70)
Number at risk
L 83 64 42 21 1
H 83 61 42 21 1
0 1,370 2,740 4,110 5,480
Overall survival(Days)
d.
HCC
RiskScore
L
H
Survival probability
p=3.0e-3
HR=3.50,95CI%(1.45,8.44)
Number at risk
L 40 26 19 8 1
H 40 32 20 12 1
0 1,370 2,740 4,110 5,480
Overall survival(Days)

Figure 6. NK cell exhaustion predicts poor prognosis of inflammatory diseases. **a.-d.** Kaplan-Meier survival curves for cholecystitis, pancreatitis, lung adenocarcinoma, and hepatocellular carcinoma according to the markers of NK cell exhaustion in the GSE166915, GSE91035, GSE75037, and GSE41804 datasets.

Figure 1

a.

Genotypes of ATP7B in 20 WD cases

Mutant alleles*	Amino acid change	No. (%)
c.2333G>T	p.R778L	13 (65%)
c.2804C>T	p.T935M	0 (0%)
c.2975C>T	p.P992L	0 (0%)
Unknow	Unknow	7 (35%)

* Reference. Seq: NM_000053.4

b.

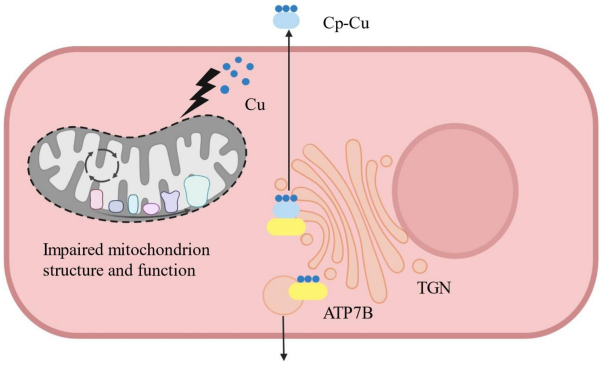

c.

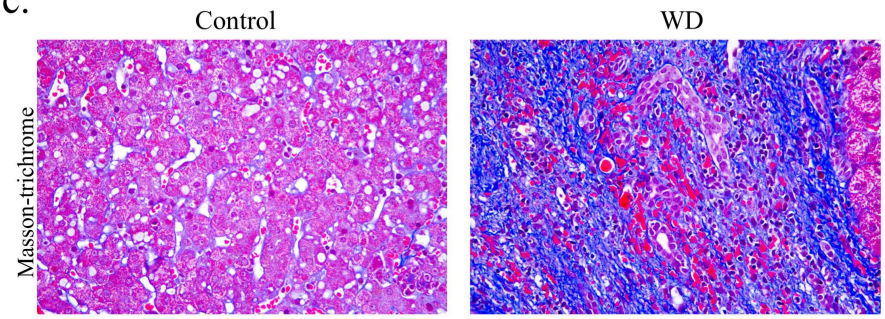

d.

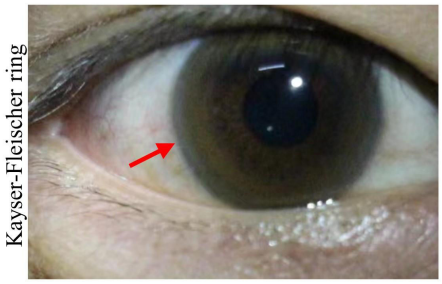

e.

Clinical statistics of the patients.

Cohort 1			
	WD (n=92)	HBV (n=95)	*P* value
TBIL - μmol/L (≤26)	14.90±6.59	20.46±13.94	0.0007
TG - μmol/L (≤1.7)	0.98±0.58	0.99±0.71	0.7699
T-CHOL - μmol/L (3-5.7)	4.09±0.75	3.84±1.13	0.0743

Cohort 2			
	WD (n=618)	HBV (n=370)	*P* value
Hyperqlycemia – no. (%)	33 (5.34%)	42 (11.35%)	0.0006
Gallstone – no. (%)	65 (10.52%)	39 (10.54%)	0.9910
Cholecystitis – no. (%)	306 (49.51%)	35 (9.46%)	0.0001

Cohort 3			
	Cholecystitis & WD (n=34)	Cholecystitis (n=44)	*P* value
WBC – no. (%)	12 (35.29%)	1 (2.27%)	0.0004
NEU – no. (%)	10 (29.41%)	5 (11.36%)	0.0449
LYM – no. (%)	11 (32.35%)	6 (13.64%)	0.0471
TBIL – no. (%)	5 (14.71%)	6 (13.64%)	0.8929
ALB – no. (%)	10 (29.41%)	10 (22.73%)	0.5026
ALT – no. (%)	18 (52.94%)	28 (63.64%)	0.3410
AST – no. (%)	9 (26.47%)	11 (25.00%)	0.8827

WD, Wilson disease; HBV, Hepatitis B virus; ; TBIL, Total bilirubin; TG, Triglyceride; T-CHOL, Total cholesterol; WBC, White blood cell; NEU, Neutrophil; LYM, Lymphocyte; ALB, Albumin; ALT, Alanine aminotransferase; AST, Aspartate aminotransferase.

Figure 2

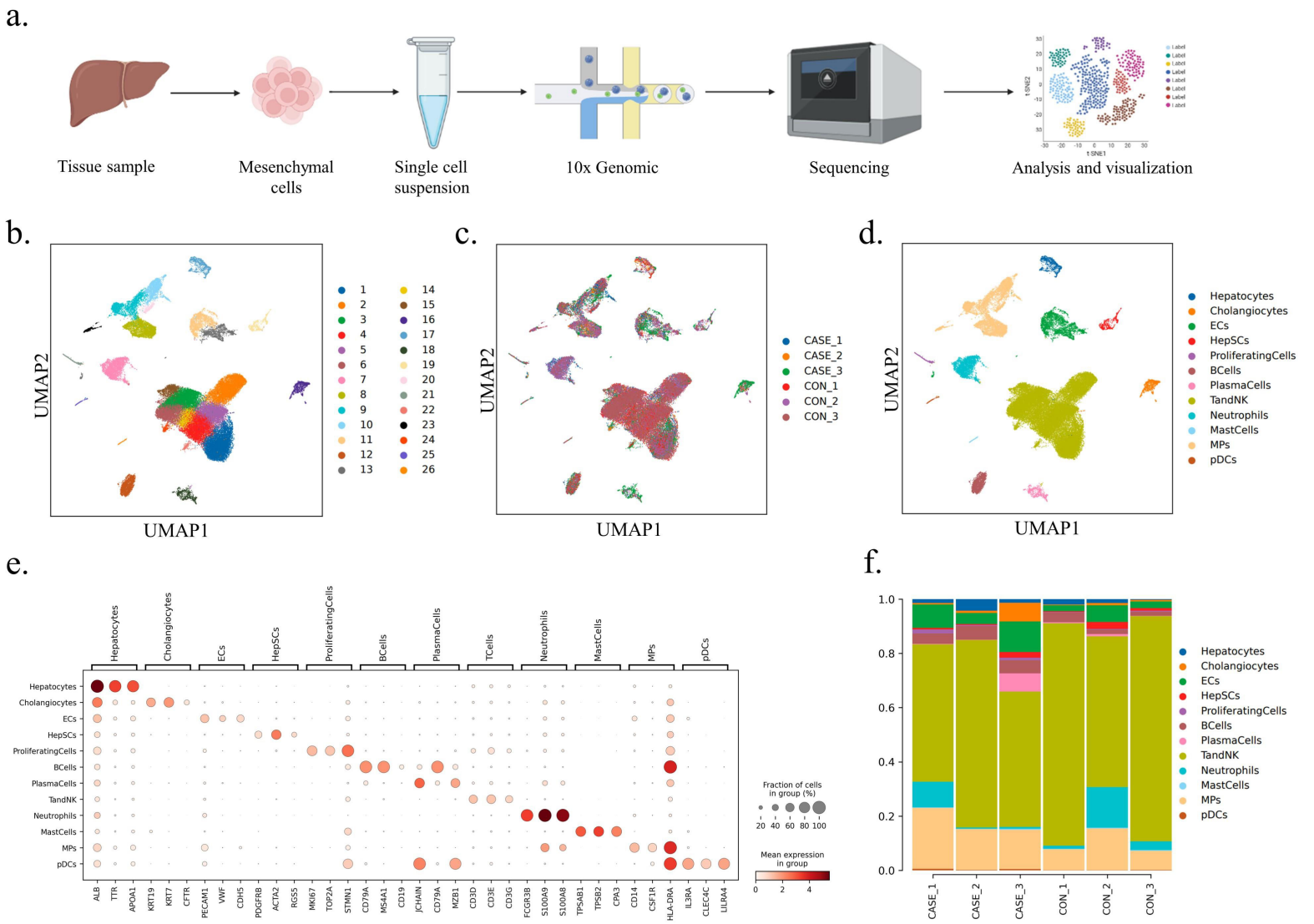
a.
Tissue sample
Mesenchymal cells
Single cell suspension
10x Genomic
Sequencing
Analysis and visualization
b.
UMAP2
UMAP1
1
2
3
4
5
6
7
8
9
10
11
12
13
14
15
16
17
18
19
20
21
22
23
24
25
26
c.
UMAP2
UMAP1
CASE_1
CASE_2
CASE_3
CON_1
CON_2
CON_3
d.
UMAP2
UMAP1
Hepatocytes
Cholangiocytes
ECs
HepSCs
ProliferatingCells
BCells
PlasmaCells
TandNK
Neutrophils
MastCells
MPs
pDCs
e.
Hepatocytes
Cholangiocytes
ECs
HepSCs
ProliferatingCells
BCells
PlasmaCells
TandNK
Neutrophils
MastCells
MPs
pDCs
ALB
TTR
APOA1
KRT19
KRT7
CFTR
PECAM1
VWF
CDH5
PDGFRB
ACTA2
RGS5
MKI67
TOP2A
STMN1
CD79A
MS4A1
CD19
JCHAIN
CD79A
MZB1
CD3D
CD3E
CD3G
FCGR3B
S100A9
S100A8
TPSAB1
TPSB2
CPA3
CD14
CSF1R
HLA-DRA
IL3RA
CLEC4C
LILRA4
Fraction of cells in group (%)
20 40 60 80 100
Mean expression in group
0 2 4
f.
1.0
0.8
0.6
0.4
0.2
0.0
CASE_1
CASE_2
CASE_3
CON_1
CON_2
CON_3
Hepatocytes
Cholangiocytes
ECs
HepSCs
ProliferatingCells
BCells
PlasmaCells
TandNK
Neutrophils
MastCells
MPs
pDCs

Figure 3

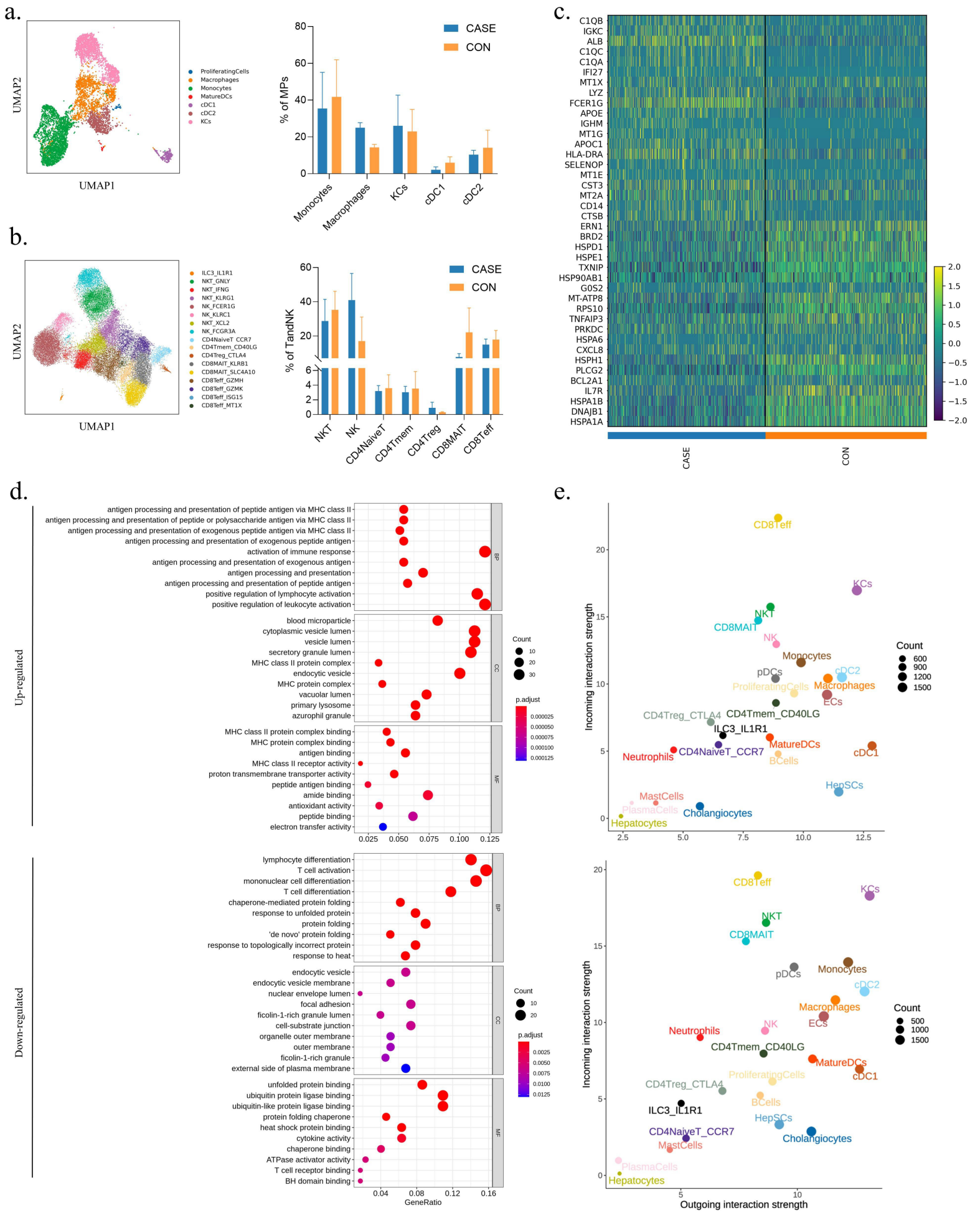
a.
UMAP2
UMAP1
ProliferatingCells
Macrophages
Monocytes
MatureDCs
cDC1
cDC2
KCs
% of MPs
CASE
CON
Monocytes
Macrophages
KCs
cDC1
cDC2
b.
UMAP2
UMAP1
ILC3_IL1R1
NKT_GNLY
NKT_IFNG
NKT_KLRG1
NK_FCER1G
NK_KLRC1
NKT_XCL2
NK_FCGR3A
CD4NaiveT_CCR7
CD4Tmem_CD40LG
CD4Treg_CTLA4
CD8MAIT_KLRB1
CD8MAIT_SLC4A10
CD8Teff_GZMH
CD8Teff_GZMK
CD8Teff_ISG15
CD8Teff_MT1X
% of TandNK
CASE
CON
NKT
NK
CD4NaiveT
CD4Tmem
CD4Treg
CD8MAIT
CD8Teff
c.
C1QB
IGKC
ALB
C1QC
C1QA
IFI27
MT1X
LYZ
FCER1G
APOE
IGHM
MT1G
APOC1
HLA-DRA
SELENOP
MT1E
CST3
MT2A
CD14
CTSB
ERN1
BRD2
HSPD1
HSPE1
TXNIP
HSP90AB1
G0S2
MT-ATP8
RPS10
TNFAIP3
PRKDC
HSPA6
CXCL8
HSPH1
PLCG2
BCL2A1
IL7R
HSPA1B
DNAJB1
HSPA1A
CASE
CON
d.
Up-regulated
antigen processing and presentation of peptide antigen via MHC class II
antigen processing and presentation of peptide or polysaccharide antigen via MHC class II
antigen processing and presentation of exogenous peptide antigen via MHC class II
antigen processing and presentation of exogenous peptide antigen
activation of immune response
antigen processing and presentation of exogenous antigen
antigen processing and presentation
antigen processing and presentation of peptide antigen
positive regulation of lymphocyte activation
positive regulation of leukocyte activation
BP
blood microparticle
cytoplasmic vesicle lumen
vesicle lumen
secretory granule lumen
MHC class II protein complex
endocytic vesicle
MHC protein complex
vacuolar lumen
primary lysosome
azurophil granule
CC
MHC class II protein complex binding
MHC protein complex binding
antigen binding
MHC class II receptor activity
proton transmembrane transporter activity
peptide antigen binding
amide binding
antioxidant activity
peptide binding
electron transfer activity
MF
Count
p.adjust
Down-regulated
lymphocyte differentiation
T cell activation
mononuclear cell differentiation
T cell differentiation
chaperone-mediated protein folding
response to unfolded protein
protein folding
'de novo' protein folding
response to topologically incorrect protein
response to heat
BP
endocytic vesicle
endocytic vesicle membrane
nuclear envelope lumen
focal adhesion
ficolin-1-rich granule lumen
cell-substrate junction
organelle outer membrane
outer membrane
ficolin-1-rich granule
external side of plasma membrane
CC
unfolded protein binding
ubiquitin protein ligase binding
ubiquitin-like protein ligase binding
protein folding chaperone
heat shock protein binding
cytokine activity
chaperone binding
ATPase activator activity
T cell receptor binding
BH domain binding
MF
GeneRatio
e.
Incoming interaction strength
CD8Teff
KCs
NKT
CD8MAIT
NK
Monocytes
pDCs
cDC2
ProliferatingCells
Macrophages
ECs
CD4Treg_CTLA4
CD4Tmem_CD40LG
ILC3_IL1R1
MatureDCs
Neutrophils
CD4NaiveT_CCR7
BCells
cDC1
HepSCs
MastCells
PlasmaCells
Cholangiocytes
Hepatocytes
Count
Outgoing interaction strength

Figure 4

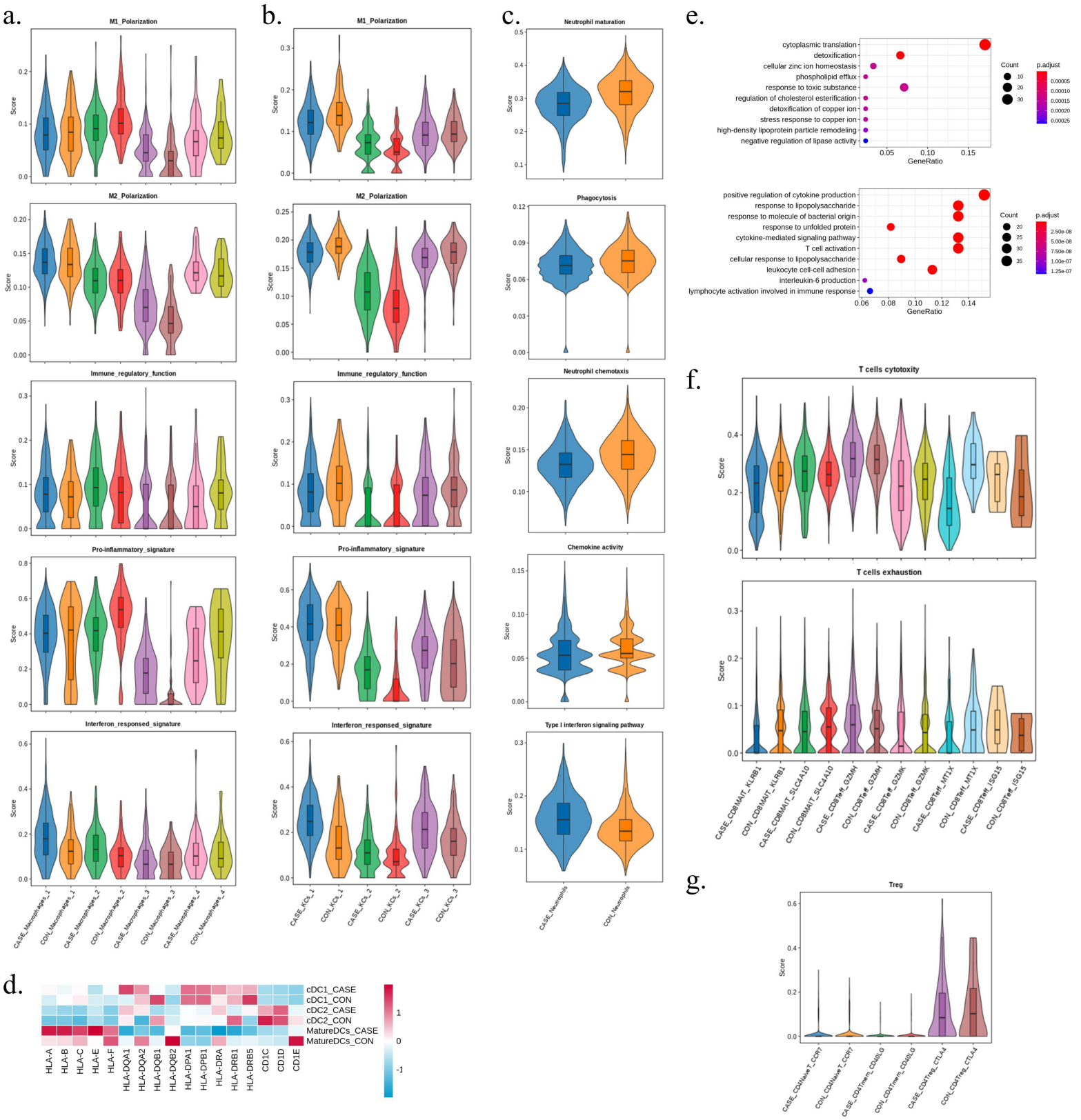
a.
M1_Polarization
M2_Polarization
Immune_regulatory_function
Pro-inflammatory_signature
Interferon_responsed_signature
Score
CASE_Macrophages_1
CON_Macrophages_1
CASE_Macrophages_2
CON_Macrophages_2
CASE_Macrophages_3
CON_Macrophages_3
CASE_Macrophages_4
CON_Macrophages_4
b.
M1_Polarization
M2_Polarization
Immune_regulatory_function
Pro-inflammatory_signature
Interferon_responsed_signature
CASE_KCs_1
CON_KCs_1
CASE_KCs_2
CON_KCs_2
CASE_KCs_3
CON_KCs_3
c.
Neutrophil maturation
Phagocytosis
Neutrophil chemotaxis
Chemokine activity
Type I interferon signaling pathway
CASE_Neutrophils
CON_Neutrophils
e.
cytoplasmic translation
detoxification
cellular zinc ion homeostasis
phospholipid efflux
response to toxic substance
regulation of cholesterol esterification
detoxification of copper ion
stress response to copper ion
high-density lipoprotein particle remodeling
negative regulation of lipase activity
GeneRatio
Count
p.adjust
positive regulation of cytokine production
response to lipopolysaccharide
response to molecule of bacterial origin
response to unfolded protein
cytokine-mediated signaling pathway
T cell activation
cellular response to lipopolysaccharide
leukocyte cell-cell adhesion
interleukin-6 production
lymphocyte activation involved in immune response
f.
T cells cytotoxity
T cells exhaustion
CASE_CD8MAIT_KLRB1
CON_CD8MAIT_KLRB1
CASE_CD8MAIT_SLC4A10
CON_CD8MAIT_SLC4A10
CASE_CD8Tef_GZMH
CON_CD8Tef_GZMH
CASE_CD8Tef_GZMK
CON_CD8Tef_GZMK
CASE_CD8Tef_MT1X
CON_CD8Tef_MT1X
CASE_CD8Tef_ISG15
CON_CD8Tef_ISG15
g.
Treg
CASE_CD4Naive T_CCR7
CON_CD4Naive T_CCR7
CASE_CD4Treg_CD40LG
CON_CD4Treg_CD40LG
CASE_CD4Treg_CTLA4
CON_CD4Treg_CTLA4
d.
cDC1_CASE
cDC1_CON
cDC2_CASE
cDC2_CON
MatureDCs_CASE
MatureDCs_CON
HLA-A
HLA-B
HLA-C
HLA-E
HLA-F
HLA-DQA1
HLA-DQA2
HLA-DQB1
HLA-DQB2
HLA-DPA1
HLA-DPB1
HLA-DRA
HLA-DRB1
HLA-DRB5
CD1C
CD1D
CD1E

Figure 5

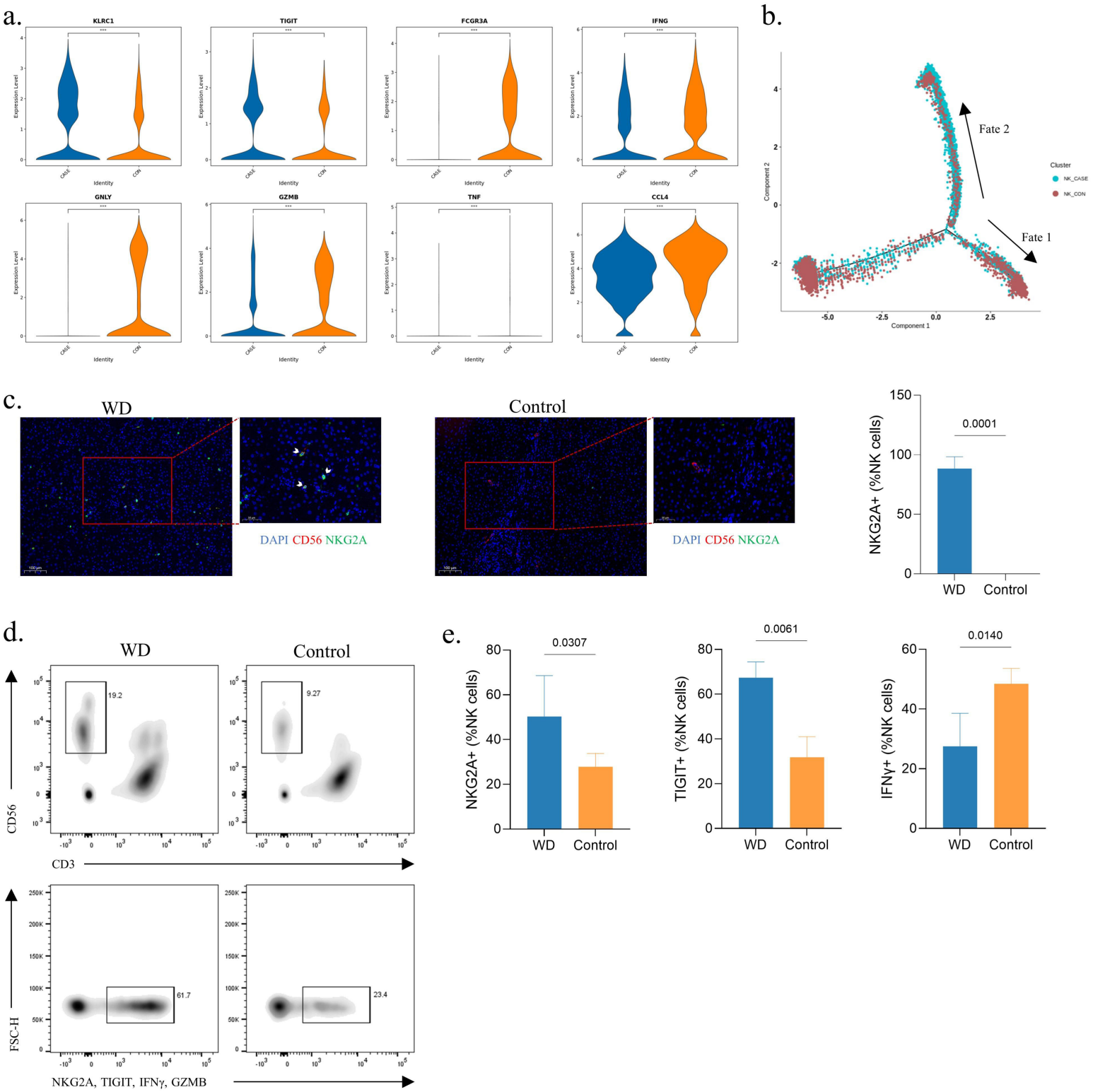
a.
KLRC1
TIGIT
FCGR3A
IFNG
GNLY
GZMB
TNF
CCL4
Expression Level
Identity
CASE
CON
b.
Fate 2
Fate 1
Cluster
NK_CASE
NK_CON
Component 1
Component 2
c.
WD
Control
DAPI CD56 NKG2A
NKG2A+ (%NK cells)
0.0001
d.
WD
Control
CD56
CD3
19.2
9.27
FSC-H
NKG2A, TIGIT, IFNγ, GZMB
61.7
23.4
e.
NKG2A+ (%NK cells)
0.0307
TIGIT+ (%NK cells)
0.0061
IFNγ+ (%NK cells)
0.0140

Figure 6

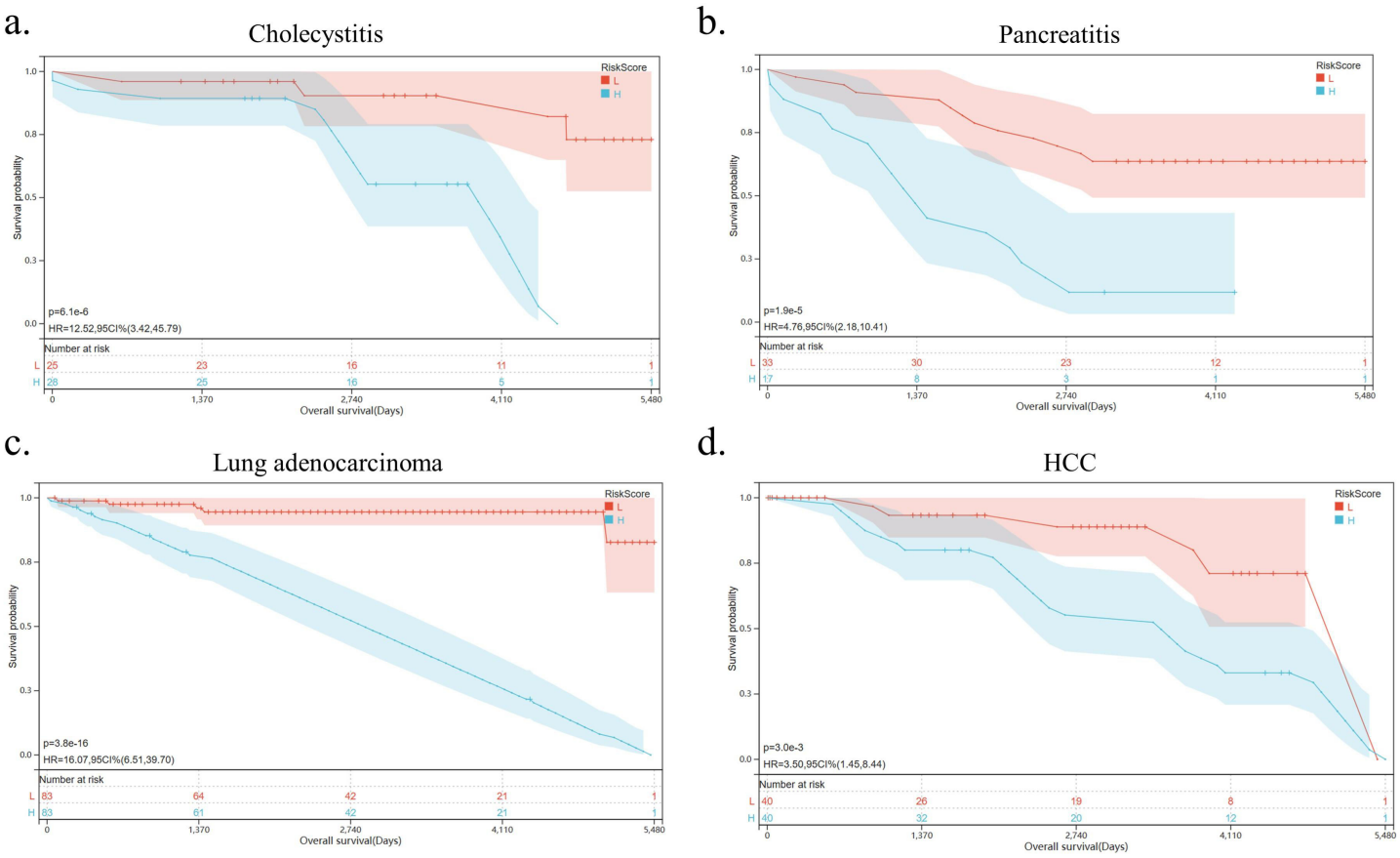
a.
Cholecystitis
RiskScore
L
H
Survival probability
1.0
0.8
0.5
0.3
0.0
p=6.1e-6
HR=12.52,95CI%(3.42,45.79)
Number at risk
L 25 23 16 11 1
H 28 25 16 5 1
0 1,370 2,740 4,110 5,480
Overall survival(Days)
b.
Pancreatitis
RiskScore
L
H
Survival probability
1.0
0.8
0.5
0.3
0.0
p=1.9e-5
HR=4.76,95CI%(2.18,10.41)
Number at risk
L 33 30 23 12 1
H 17 8 3 1 1
0 1,370 2,740 4,110 5,480
Overall survival(Days)
c.
Lung adenocarcinoma
RiskScore
L
H
Survival probability
1.0
0.8
0.5
0.3
0.0
p=3.8e-16
HR=16.07,95CI%(6.51,39.70)
Number at risk
L 83 64 42 21 1
H 83 61 42 21 1
0 1,370 2,740 4,110 5,480
Overall survival(Days)
d.
HCC
RiskScore
L
H
Survival probability
1.0
0.8
0.5
0.3
0.0
p=3.0e-3
HR=3.50,95CI%(1.45,8.44)
Number at risk
L 40 26 19 8 1
H 40 32 20 12 1
0 1,370 2,740 4,110 5,480
Overall survival(Days)